Article

Neuron

A Neural Circuit Mechanism for Encoding Aversive Stimuli in the Mesolimbic Dopamine System

Graphical Abstract

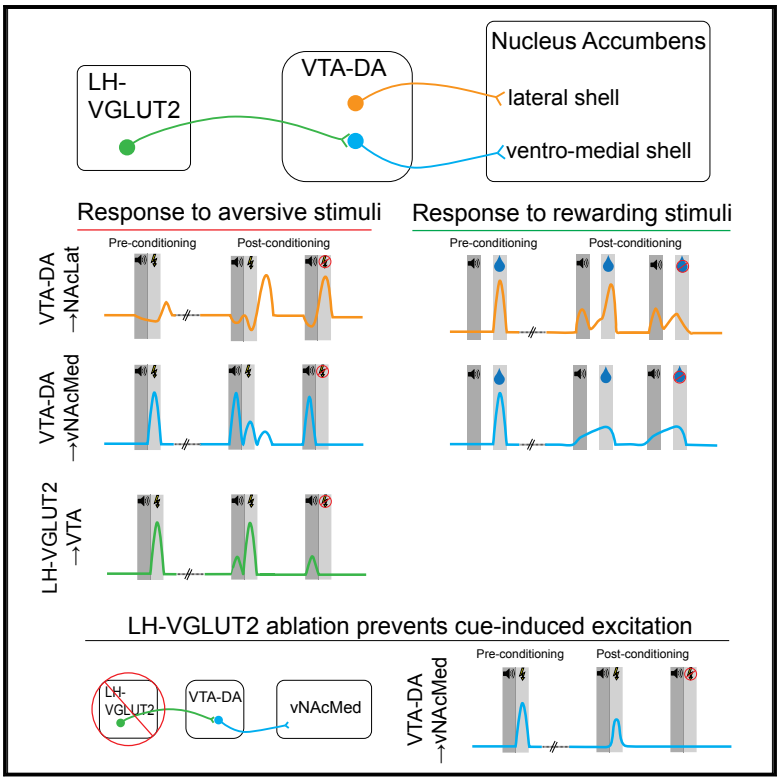

Highlights

- DA terminals in ventral NAc medial shell (vNAcMed) are excited by aversive stimuli
- DA terminals in all other NAc subregions are inhibited by aversive stimuli
- Excitation to reward-predictive cues is absent in vNAcMed DA terminals
- DA→vNAcMed neurons encode aversive-predicting stimuli through LH-VGLUT2 inputs

Authors

Johannes W. de Jong, Seyedeh Atiyeh Afjei, Iskra Pollak Dorocic, ..., Lin Tian, Karl Deisseroth, Stephan Lammel

Correspondence

lammel@berkeley.edu

In Brief

The mesolimbic dopamine system plays an important role in reward, reinforcement learning and motivated behaviors. de Jong et al. reveal a circuit mechanism that implicates a subtype of mesolimbic dopamine neurons in the encoding of aversive-predicting stimuli.

de Jong et al., 2019, Neuron *101*, 133–151
January 2, 2019
https://doi.org/10.1016/j.neuron.2018.11.005

CellPress

Neuron
Article

A Neural Circuit Mechanism for Encoding Aversive Stimuli in the Mesolimbic Dopamine System

Johannes W. de Jong,[1,6] Seyedeh Atiyeh Afjei,[1,6] Iskra Pollak Dorocic,[1] James R. Peck,[1] Christine Liu,[1] Christina K. Kim,[2] Lin Tian,[3] Karl Deisseroth,[4,5] and Stephan Lammel[1,7,*]
[1]Department of Molecular and Cell Biology and Helen Wills Neuroscience Institute, University of California, Berkeley, Berkeley, CA 94720, USA
[2]Neuroscience Program, Stanford University, Stanford, CA 94305, USA
[3]Department of Biochemistry and Molecular Medicine, School of Medicine, University of California, Davis, Davis, CA 95616, USA
[4]Departments of Bioengineering and Psychiatry, Stanford University, Stanford, CA 94305, USA
[5]Howard Hughes Medical Institute, USA
[6]These authors contributed equally
[7]Lead Contact
*Correspondence: lammel@berkeley.edu
https://doi.org/10.1016/j.neuron.2018.11.005

SUMMARY

Ventral tegmental area (VTA) dopamine (DA) neurons play a central role in mediating motivated behaviors, but the circuitry through which they signal positive and negative motivational stimuli is incompletely understood. Using *in vivo* fiber photometry, we simultaneously recorded activity in DA terminals in different nucleus accumbens (NAc) subnuclei during an aversive and reward conditioning task. We find that DA terminals in the ventral NAc medial shell (vNAcMed) are excited by unexpected aversive outcomes and to cues that predict them, whereas DA terminals in other NAc subregions are persistently depressed. Excitation to reward-predictive cues dominated in the NAc lateral shell and was largely absent in the vNAcMed. Moreover, we demonstrate that glutamatergic (VGLUT2-expressing) neurons in the lateral hypothalamus represent a key afferent input for providing information about aversive outcomes to vNAcMed-projecting DA neurons. Collectively, we reveal the distinct functional contributions of separate mesolimbic DA subsystems and their afferent pathways underlying motivated behaviors.

INTRODUCTION

Ventral tegmental area (VTA) dopamine (DA) neurons serve a central role in motivated behavior and reward processing (Berridge and Kringelbach, 2015; Berridge and Robinson, 1998; Schultz, 2016; Watabe-Uchida et al., 2017; Wise, 2004; Wise and Rompre, 1989). While there is strong evidence that VTA DA neurons signal reward prediction errors, i.e., they are excited in response to rewards and reward-predicting cues and are inhibited by aversive events (Fiorillo, 2013; Keiflin and Janak, 2015; Schultz, 2016; Watabe-Uchida et al., 2017), it remains uncertain whether all VTA DA neurons, independent of their projection targets, serve this single function (Bromberg-Martin et al., 2010; Hu, 2016; Lammel et al., 2014; Roeper, 2013). Indeed, electrophysiological studies in primates and other species have identified separate populations of VTA DA neurons that are excited by aversive stimuli, leading to the hypothesis that these DA neurons may signal motivational salience rather than value (Brischoux et al., 2009; Bromberg-Martin et al., 2010). However, a major limitation of previous single-unit recording work is that the projection target of recorded VTA DA neurons was not known. Thus, despite strong evidence that VTA DA neurons can be separated anatomically, molecularly, and functionally into heterogeneous subpopulations (Bromberg-Martin et al., 2010; Gantz et al., 2018; Lammel et al., 2014; Lerner et al., 2016; Morales and Margolis, 2017; Roeper, 2013), the precise circuitry that supports value and salience coding remains largely unknown.

The mesolimbic DA system, which is comprised of VTA DA neurons projecting to the nucleus accumbens (NAc), is associated with reward, appetitive motivation, and hedonic processes, but a large body of literature suggests that it is also involved in aversion-related behaviors (Berridge and Kringelbach, 2008; Brooks and Berns, 2013; Salamone, 1994; Salamone and Correa, 2012; Salamone et al., 2005). For example, a number of different aversive stimuli (e.g., shock, tail pinch) can increase DA release in the NAc as measured by microdialysis or fast-scan cyclic voltammetry (Abercrombie et al., 1989; Anstrom et al., 2009; Badrinarayan et al., 2012; Bassareo et al., 2002; Budygin et al., 2012; Deutch and Cameron, 1992; Martinez et al., 2008; Young, 2004). It is unclear, however, whether there is a separate subpopulation of mesolimbic DA neurons that responds differentially to appetitive and aversive stimuli.

By using *in vivo* fiber photometry, we simultaneously recorded calcium activity in DA terminals in distinct NAc subnuclei during an aversive and reward conditioning task. The advantage of this approach is that fluorescence activity signals can be recorded from DA terminals in separate NAc subdivisions, thereby directly comparing projection- and cell-type-specific activity dynamics under the same experimental conditions and in the same animal. Because the neurochemical identity and source of the inputs may play an important role for modulation of DA neuron firing

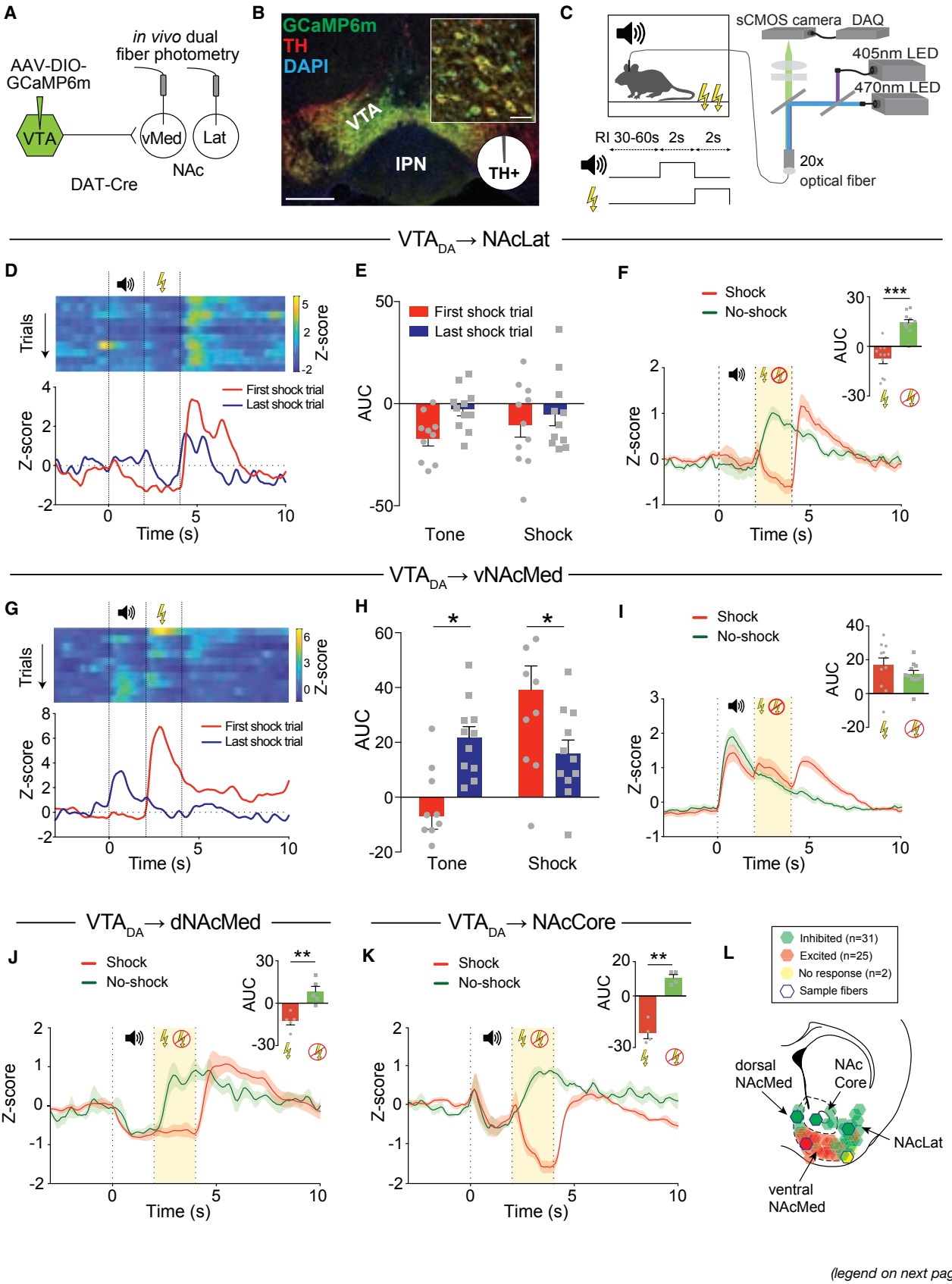

(legend on next page)

in response to motivational stimuli, we also explored the identity and function of VTA afferents that may provide aversion-related information to mesolimbic DA subpopulations.

RESULTS

Functional Topography of Aversion Encoding in the Mesolimbic DA System

We targeted the calcium indicator GCaMP6m to VTA DA neurons by injecting a Cre-dependent adeno-associated virus (AAV) encoding GCaMP6m into the VTA of dopamine transporter (DAT)-Cre driver mice and implanted optical fibers in the nucleus accumbens lateral shell (NAcLat) and nucleus accumbens medial shell (NAcMed) of the same animal (Figure 1A). Immunohistochemical analysis revealed that 99.8% of the VTA neurons that expressed GCaMP6m were also immunopositive for tyrosine hydroxylase (TH), suggesting that GCaMP6m was almost exclusively expressed in VTA DA neurons (Figure 1B; n = 234/236 cells, n = 4 mice). Because NAcMed-targeted optical fibers were specifically located in the ventral part of the NAcMed, we will refer to the ventral NAcMed (vNAcMed) from now on. We then recorded calcium transients at axon terminals simultaneously in the vNAcMed and NAcLat, while the animals received a series of tone-shock pairings. On a random interval schedule (30- to 60-s inter-trial interval), mice received a 2-s tone (conditioned stimulus, CS), which was followed by a 2-s electrical foot shock (unconditioned stimulus, US; Figure 1C). Freezing behavior of the animals significantly increased following repeated exposure to the CS (Figure S1A), indicating that an association was learned between the CS and US.

Consistent with previous electrophysiological studies demonstrating that most DA neurons are inhibited by aversive stimuli (Mirenowicz and Schultz, 1996; Ungless et al., 2004), we observed a decrease in DA terminal activity in the NAcLat in response to both US and CS (Figures 1D, 1E, and S1B; Video S1; tone: first: −17.36 ± 3.35; last: −2.79 ± 3.15; shock: first: −10.37 ± 6.03; last: −5.23 ± 5.6, n = 11 mice; two-way repeated measures [RM] ANOVA: no effect). Notably, while activity decreased during the shock, we noted a robust increase following its termination (Figure 1F). In addition, in trials in which a predicted shock was omitted, activity in NAcLat DA terminals increased significantly (Figure 1F; shock: −7.3 ± 2.88, no-shock: 14.3 ± 1.89, n = 11 mice; $p < 0.001$, paired Student's t test). In contrast, an US increased DA terminal activity in the vNAcMed initially, but the response decreased in subsequent trials and was ~2 times smaller after conditioning. Strikingly, the response of DA terminals in the vNAcMed to the CS was significantly increased after conditioning (Figures 1G, 1H, and S1C; Video S1; tone: first: −6.95 ± 4.74; last: 21.62 ± 4.12; shock: first: 39.23 ± 8.69; last: 15.90 ± 4.95, n = 11 mice; two-way RM ANOVA interaction $p < 0.01$, Holm-Sidak post hoc test, $p < 0.05$). Omission of a predicted shock resulted in a significantly smaller peak at the time of predicted shock onset; this difference was not immediately apparent from area under the curve (AUC) analysis due to the large increase and slow decline in CS-evoked activity (Figure 1I; shock: 16.93 ± 4.14; no-shock: 11.64 ± 2.09, n = 11 mice; $p = 0.18$, paired Student's t test) but was evident when we analyzed the signal amplitude at onset of the shock and its omission (Figure S1D).

Given that our recordings were performed in the vNAcMed, we also implanted optical fibers targeting the dorsal NAcMed (dNAcMed) or NAcCore in separate cohorts of mice. Notably, foot shock and its omission induced neural activity dynamics in both dNAcMed (Figure 1J; shock: −12.7 ± 2.69; no-shock: 8.16 ± 3.79, n = 5 mice; $p = 0.010$, paired Student's t test) and NAcCore (Figure 1K; shock: −21.3 ± 3.3;

Figure 1. VTA DA Terminals in Distinct NAc Subregions Show Different Responses to Aversive Stimuli

(A) Schematic of experimental design.

(B) GCaMP6m (green), tyrosine hydroxylase (TH; red), and DAPI (blue) immunofluorescence in the VTA (IPN, interpeduncular nucleus; scale bar, 500 μm). Inset pie chart: 99.8% of the VTA neurons that expressed GCaMP6m were also immunopositive for TH. Inset fluorescence image shows higher magnification (scale bar, 20 μm).

(C) Schematic of aversive conditioning procedure and fiber photometry setup (RI, random interval).

(D) Top: representative heatmaps for NAcLat DA terminals showing individual *Z* scores for trials in which a 2-s tone was followed by a 2-s electrical foot shock (first to last shock trial). Bottom: example of responses to the tone and foot shock before (first shock trial, red) and after conditioning (last shock trial, blue).

(E) Before (first shock trial, red) and after conditioning (last shock trial, blue), both tone and foot shock decrease DA terminal activity in the NAcLat (quantified as area under the curve, AUC, during each 2-s epoch; data represent means ± SEM).

(F) Comparison of *Z* score averages for NAcLat GCaMP6m fluorescence for trials in which a tone was followed by a foot shock (red) or was omitted (green; experiments were performed 24 hr after conditioning and consisted of 30 trials; 10 out of 30 tones (randomly assigned) were not followed by an electric foot shock; 67% foot shock probability). Inset shows significant increase in activity (quantified as AUC) in no-shock trials compared with shock trials (***$p < 0.001$; data represent means ± SEM).

(G) Top: representative heat maps for vNAcMed DA terminals showing individual *Z* scores for trials in which a 2-s tone was followed by a 2-s electrical foot shock (first to last shock trial). Bottom: example of responses to the tone and foot shock before (first shock trial, red) and after conditioning (last shock trial, blue).

(H) Before (first shock trial, red) and after conditioning (last shock trial, blue), after conditioning, both tone and foot shock increase DA terminal activity in the vNAcMed (*$p < 0.05$; quantified as area under the curve, AUC, during each 2-s epoch; data represent means ± SEM).

(I) Comparison of Z score averages for vNAcMed GCaMP6m fluorescence for trials in which a tone was followed by a foot shock (red) or was omitted (green; experiments were performed 24 hr after conditioning and consisted of 30 trials; 10 out of 30 tones (randomly assigned) were not followed by an electric foot shock; 67% foot shock probability). Inset shows activity (quantified as AUC) in no-shock trials compared with shock trials. Note that, although quantification of AUC does not yield significant differences between shock and no-shock conditions, a peak is observed following shock onset, which is absent in no-shock trials (Figure S1D; *$p < 0.05$; data represent means ± SEM).

(J and K) Comparison of *Z* score averages for DA terminals in the dorsal NAcMed (dNAcMed; J) and NAcCore (K) in response to shock (red) and omission (green) trials. Inset shows AUC during shock versus no-shock trials (**$p < 0.01$; data represent means ± SEM).

(L) Schematic of the anatomical locations of individual optical fiber implants from all animals. Different colors indicate the response to foot shock (red, excitation; green, inhibition; yellow, no response; blue hexagons highlight the examples shown in Figure S1E).

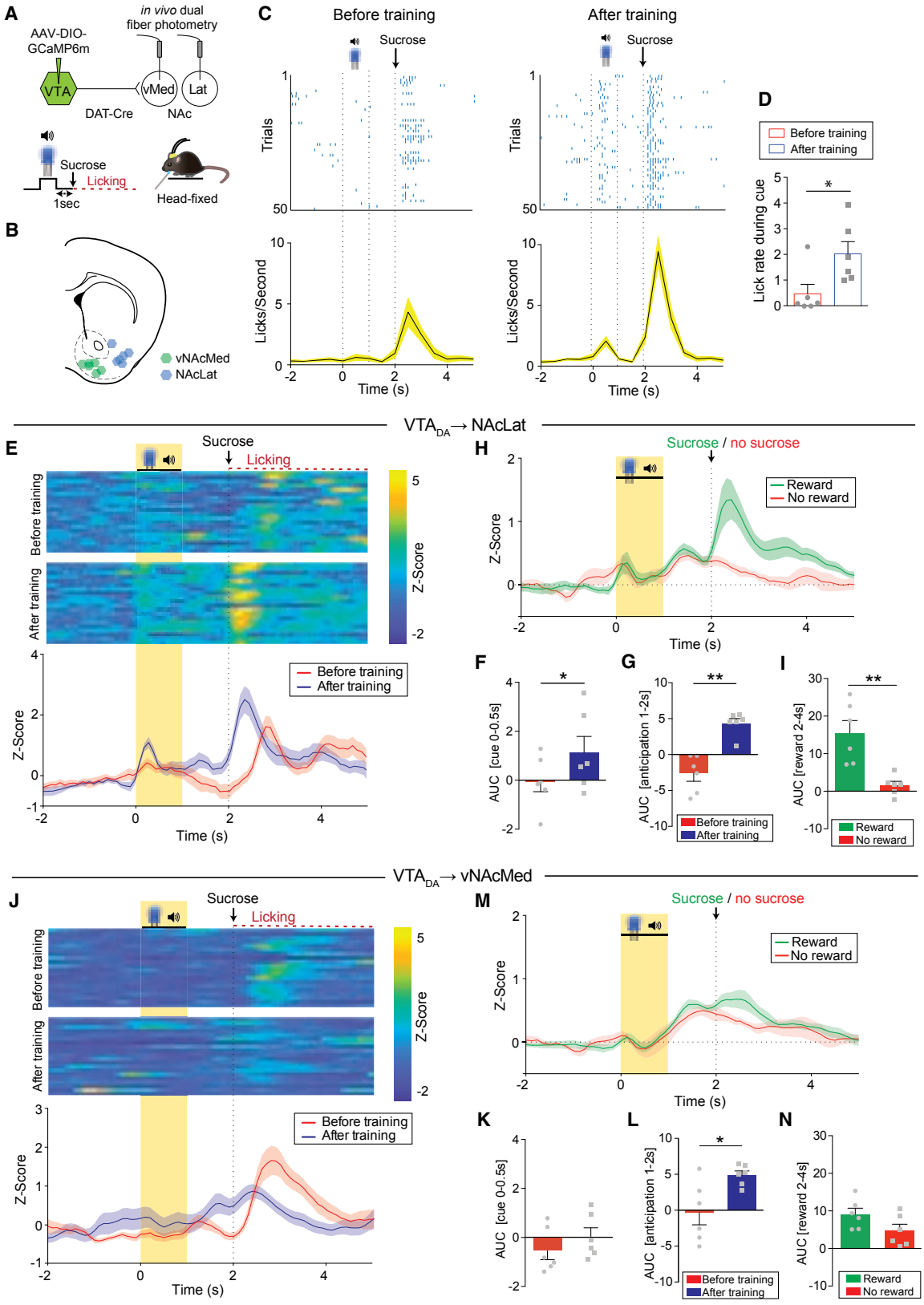

(legend on next page)

no-shock: 10.59 ± 1.87, n = 4 mice; p = 0.008 paired Student's t test) DA terminals that were similar to NAcLat. Collectively, anatomical and functional analysis of 58 recording sites from 33 mice suggests a remarkable topographic organization of aversive DA signaling in the NAc (Figures 1L and S1E).

Excitatory Responses to Reward-Predictive Cues Dominate in NAcLat DA Terminals

To investigate whether DA terminals in the vNAcMed are activated solely by aversive stimuli or rather signal motivational salience, we subjected a subset of mice (n = 6) that underwent the aversive conditioning procedure to a Pavlovian reward conditioning paradigm (Figures 2A and 2B). We presented a 1-s cue (light and tone) followed by a 1-s delay and delivery of a sucrose solution to head-fixed mice and recorded calcium activity in the vNAcMed and NAcLat. Learning that the cue predicted sucrose delivery was demonstrated by steady increases in anticipatory licking behavior and a significant increase in lick rate after conditioning (Figures 2C and 2D; session 1: 0.48 ± 0.37, session 5: 2.02 ± 0.47, n = 6 mice, p = 0.045, paired Student's t test). We found that NAcLat DA terminals lacked a coherent response to the cue early in training but showed a robust increase to reward delivery. As training progressed, most animals developed a transient increase in activity in response to the reward predictive cue (Figures 2E, 2F, and S2A; before: −0.05 ± 0.44, after: 1.13 ± 0.66, n = 6 mice, p = 0.015, paired Student's t test). Strikingly, while vNAcMed DA terminal activity initially increased in response to (unpredicted) reward delivery in a similar manner as in the NAcLat, there was no detectable response to the reward-predictive cue even after extensive training (i.e., 5 sessions of 100 trials; 500 trials in total) (Figures 2J, 2K, and S2B; before: −0.57 ± 0.37, after: 0.02 ± 0.37, n = 6 mice, p = 0.41, paired Student's t test). Moreover, both NAcLat and vNAcMed DA terminal activity increased during reward anticipation, and the response grew in magnitude as training progressed (Figures 2E, 2G, 2J, and 2L; NAcLat before: −2.43 ± 0.91, NAcLat after: 4.34 ± 0.65, n = 6 mice, p = 0.0041, paired Students' t test, vNAcMed before: −0.34 ± 1.7, vNAcMed after: 4.88 ± 0.59, n = 6 mice, p = 0.03 paired Students' t test). We also explored NAcLat and vNAcMed DA terminal activity during trials in which a predicted reward was omitted. We found that in the NAcLat there was a significant difference between the response to a predicted reward and reward omission (Figures 2H and 2I; reward: 15.53 ± 3.28, omission: 1.57 ± 1.09, n = 6 mice, p = 0.0077, paired Student's t test). Conversely, there was no significant difference between predicted reward and reward omission in the vNAcMed (Figures 2M and 2N; reward: 9.11 ± 1.6, omission: 4.71 ± 1.73, n = 6 mice, p = 0.16 paired Student's t test). Taken together, although vNAcMed DA terminals are activated by salient (i.e., appetitive and aversive) motivational stimuli, excitation to reward-predictive cues dominates in the NAcLat and is largely absent in the vNAcMed.

DR_{VGLUT3} Inputs to VTA Activate NAcLat-Projecting DA Neurons and Promote Reward

DA burst firing is highly regulated by glutamatergic inputs (Grace and Bunney, 1984). In addition, phasic increases in DA activity to motivational stimuli appear to be triggered by direct excitation, rather than disinhibition (Watabe-Uchida et al., 2017). We therefore sought to identify and characterize glutamatergic inputs to vNAcMed-projecting DA neurons that may activate these cells in response to aversive stimuli. We combined a rabies virus-based genetic mapping strategy (Figure 3A) with a semi-automated whole-brain mapping algorithm (Figures S3A–S3C). Analysis of the starter cell populations in the VTA shows that vNAcMed- and NAcLat-projecting starter cells were consistent with the topographic organization reported previously (Lammel et al., 2008), and all starter cells were TH immunopositive (Figures 3B, S3D, and S3E). Consistent with Beier et al. (2015), we identified the dorsal raphe (DR) and the lateral hypothalamus (LH) as the most prominent inputs to both vNAcMed- and NAcLat-projecting DA neurons (Figures 3B–3D; Table S1A). We first focused on the DR because of its particularly strong input to vNAcMed-projecting DA neurons. To examine whether excitatory DR neurons make functional synaptic connections onto different mesolimbic DA subtypes, we combined dual retrograde tracing and *ex vivo* electrophysiology (Figure 3E). Notably, following Cre-dependent expression of channelrhodopsin-2

Figure 2. Phasic Responses to Reward-Predictive Cues Dominate in NAcLat DA Terminals

(A) Schematic of experimental design.

(B) Schematic of fiber implant locations in the vNAcMed and NAcLat.

(C) Top: representative raster plot of licks around cue presentation and reward delivery in the first 50 trials before (first session, left) and after training (fifth session, right). Bottom: average lick rate of all mice during the first 50 trials of the first (left) and fifth session (right; data represent means ± SEM).

(D) Average lick rate during cue presentation (*p < 0.05; data represent means ± SEM).

(E) Top: representative heatmaps for NAcLat DA terminals showing individual *Z* scores during the first 20 successful trials before (first session, above) and after training (fifth session, below). Bottom: *Z* score averages of the above heatmaps (data represent means ± SEM).

(F) Mean response to the CS before (red) and after (blue) training (*p < 0.05; quantified as AUC during cue onset; data represent means ± SEM).

(G) Mean AUC during reward anticipation (delay period) before (red) and after (blue) training (**p < 0.01; data represent means ± SEM).

(H) Comparison of *Z* score averages for NAcLat GCaMP6m fluorescence during reward (green) and omission trials (red; 80% reward probability; data represent mean ± SEM); recorded during the last conditioning day (day 5).

(I) Mean AUC during reward delivery (quantified as AUC) for reward (green) and omission (red) trials (**p < 0.01; data represent means ± SEM).

(J) Top: representative heat maps for vNAcMed DA terminals showing individual *Z* scores during the first 20 successful trials before (first session, above) and after training (fifth session, below). Bottom: *Z* score averages of the above heat maps (data represent means ± SEM).

(K) Mean response to the CS before (red) and after (blue) training (data represent means ± SEM).

(L) Mean AUC during reward anticipation (delay period) before (red) and after (blue) training (*p < 0.05; data represent means ± SEM).

(M) Comparison of *Z* score averages for vNAcMed GCaMP6m fluorescence during reward (green) and omission trials (red; 80% reward probability; data represent mean ± SEM); recorded during the last conditioning day (day 5).

(N) Mean AUC during reward delivery (quantified as AUC) for reward (green) and omission (red) trials (Data represent means ± SEM).

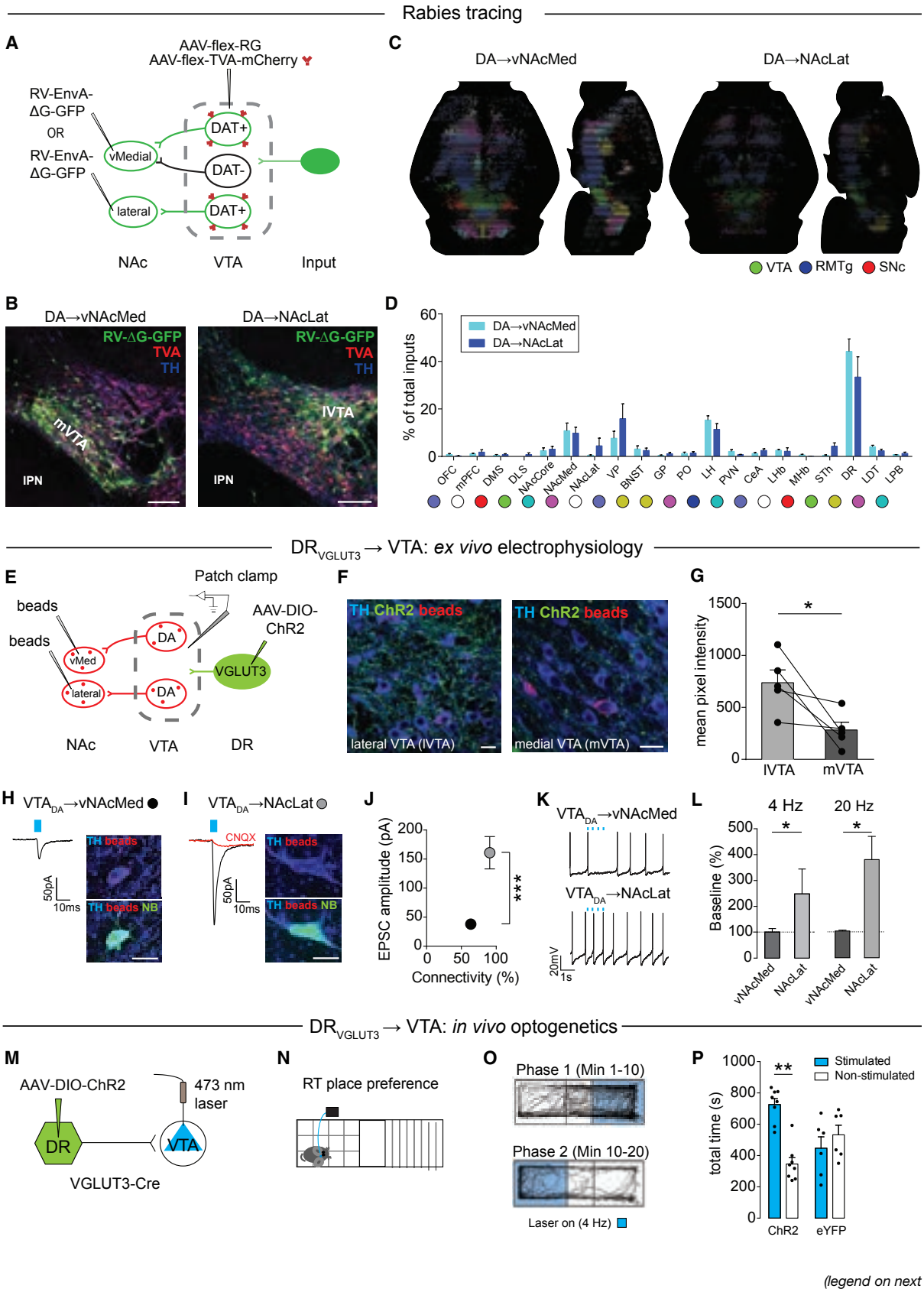

(legend on next page)

(ChR2) in glutamatergic (i.e., VGLUT3-expressing) DR neurons (DR_{VGLUT3}), ChR2 expression levels were almost 3 times higher in the lateral VTA adjacent to NAcLat-projecting DA neurons than in the medial VTA, where vNAcMed-projecting DA neurons are located (Figures 3F and 3G; lateral VTA [lVTA]: 738.6 ± 121.5, medial VTA [mVTA]: 283.2 ± 74.98, n = 5 mice, p = 0.047, paired Student's t test). Stimulation of ChR2-expressing DR_{VGLUT3} terminals produced excitatory postsynaptic currents (EPSCs) more frequently and with ~4 times larger amplitudes in NAcLat- than in vNAcMed-projecting DA neurons (Figures 3H–3J; vNAcMed: 44.82 ± 7.25 pA, n = 25/36 cells (69.4%); NAcLat: 160.90 ± 27.98 pA, n = 29/32 cells (90.6%), 28 mice, p < 0.001, Mann-Whitney test). Light-evoked EPSCs were blocked by an AMPA (α-amino-3-hydroxy-5-methyl-4-isoxazole propionic acid) receptor antagonist (10 μM 6-cyano-7-nitroquinoxaline-2,3-dione [CNQX]), indicating that DR terminals released glutamate (Figure 3I; red trace: EPSCs after bath application of CNQX; baseline: 123.1 ± 26.04 pA, CNQX: 14.35 ± 3.32 pA, n = 6 cells, 3 mice, p < 0.01, paired Student's t test). Importantly, NAcLat- but not vNAcMed-projecting DA neurons, both recorded in the same set of slices, significantly increased firing in response to both 4- and 20-Hz optical stimulation of DR_{VGLUT3} inputs (Figures 3K and 3L; 4 Hz: vNAcMed: 102 ± 9.87%, n = 8 cells; NAcLat: 246 ± 89.78%, n = 16 cells, p = 0.013, Mann-Whitney test; 20 Hz: vNAcMed: 103.5 ± 3.17%, n = 7 cells; NAcLat: 379.4 ± 89.54%, n = 14 cells, 7 mice, p = 0.012, Mann-Whitney test). If DR_{VGLUT3} neurons preferentially activate reward-encoding NAcLat-projecting DA neurons (Figure 2), then it is reasonable to assume that activation of DR_{VGLUT3} terminals in the VTA would promote reward-related behavior. Indeed, consistent with other studies (Liu et al., 2014; McDevitt et al., 2014; Qi et al., 2014), we found that stimulation of DR_{VGLUT3} terminals in the VTA induced robust place preference behavior (Figures 3M–3P; ChR2: stimulated [stim.]: 725.9 ± 37.6 s, non-stimulated [non-stim.]: 345.9 ± 40.3 s, n = 8 mice; enhanced yellow fluorescent protein [eYFP]: stim.: 447 ± 72.85 s, non-stim.: 532.5 ± 61.15 s, n = 6 mice; two-way RM ANOVA interaction p < 0.01, Holm-Sidak post hoc test, p < 0.01). Taken together, DR_{VGLUT3} neurons predominantly target NAcLat-projecting DA neurons and activation of this pathway promotes reward. Thus, it is unlikely that DR_{VGLUT3} inputs contribute to the aversion-related excitation of vNAcMed-projecting DA neurons.

Bidirectional Modulation of Aversive Behavior by LH_{VGLUT2} Inputs to VTA

We next focused on LH inputs because subpopulations of LH neurons have been associated with aversive states (Ball, 1970; Schwartzbaum and Leventhal, 1990). Indeed, a recent optogenetic study has suggested a potential role for excitatory LH inputs to the VTA in mediating aversive-related behaviors (Nieh et al., 2016), though some controversy on this subject remains as another study found that optical self-stimulation of excitatory LH to VTA synapses is rewarding (Kempadoo et al., 2013).

We sought to re-examine these previous findings (Kempadoo et al., 2013; Nieh et al., 2016) and test whether activation of excitatory LH inputs to the VTA promotes aversion- or reward-related behaviors. To do this, we injected a Cre-dependent, AAV double-floxed–inverse open reading frame–encoding ChR2 (AAV-DIO-ChR2) into the LH of VGLUT2-Cre mice and implanted an optical fiber dorsal to the VTA (Figures 4A, 4B, and S4A). 8 weeks later, we performed a real-time place preference assay (Figure 4C). We found that 4-Hz optogenetic stimulation of glutamatergic (i.e., VGLUT2-expressing) LH (LH_{VGLUT2}) terminals in the VTA caused robust real-time place aversion (Figures 4D–4F; Video S2; ChR2: stim.: 315.6 ± 14.29 s, non-stim.: 537.2 ± 37.37 s, n = 7 mice; eYFP: stim.: 418.8 ± 73.56 s, non-stim.: 421.3 ± 46.03 s, n = 6 mice; two-way RM ANOVA interaction p < 0.05, Holm-Sidak post hoc test, p < 0.01). Place aversion behavior was frequency dependent; while 1-Hz optogenetic stimulation had no effect, 20-Hz stimulation induced the strongest place aversion behavior (Figures S5A–S5G). Optogenetic stimulation of LH_{VGLUT2} terminals in the VTA had no effects on locomotion in

Figure 3. DR_{VGLUT3} Inputs to VTA Activate NAcLat-Projecting DA Neurons and Promote Reward

(A) Schematic of experimental design.

(B) Anatomical distribution of vNAcMed- (left) and NAcLat-projecting (right) starter cells. Note the clear anatomical separation of the two subtypes and their locations in the mVTA (mVTA) and lateral VTA (lVTA), respectively (green, RV-ΔG-GFP; red, TVA-mCherry; blue, TH; scale bar, 25 μm).

(C) Horizontal and sagittal views of processed whole brains displaying brain-wide inputs to vNAcMed- (left) and NAcLat- (right) projecting DA neurons.

(D) Quantification of inputs to vNAcMed- (light blue) and NAcLat- (dark blue) projecting DA neurons. Data are presented as a percentage of total input (px) counted in each individual brain. Color code indicates different brain structures shown in (C). Abbreviations shown in legend of Figure S3 (data represent means ± SEM).

(E) Schematic of experimental design.

(F) ChR2-eYFP expressing DR_{VGLUT3} terminals (green) are more frequently detected in the lVTA adjacent to retrogradely labeled (beads, red) TH-immunopositive (blue) cells projecting to NAcLat (left) than in the mVTA (right; scale bars, 10 μm).

(G) Mean fluorescence intensity of ChR2-eYFP expression in lVTA and mVTA (*p < 0.05; data represent means ± SEM).

(H and I) EPSCs generated by stimulation of DR_{VGLUT3} inputs in retrogradely labeled (beads, red) VTA neurons projecting to (H) vNAcMed or (I) NAcLat. Cells were filled with neurobiotin (NB, green) and are TH immunopositive (blue; scale bars, 50 pA/10 ms, 10 μm; data represent means ± SEM).

(J) Mean EPSC amplitudes and response probabilities generated by light stimulation of DR_{VGLUT3} inputs (***p < 0.001; data represent means ± SEM).

(K) Spontaneous firing in vNAcMed- (top) and NAcLat-projecting (bottom) DA neurons and 4-Hz stimulation of DR_{VGLUT3} inputs (scale bar, 20 mV/1 s).

(L) Relative increase in firing rate during 4- and 20-Hz DR_{VGLUT3} terminal stimulation for vNAcMed- and NAcLat-projecting DA neurons (*p < 0.05; data represent means ± SEM).

(M) Schematic of experimental design.

(N) Schematic of real-time place preference assay.

(O) Trajectory of an animal that received 4-Hz light stimulation in one compartment (phase 1, blue, top panel) for the initial 10-min period followed by stimulation in the other compartment (phase 2, blue, lower panel) for an additional 10 min.

(P) Mean time mice spent in the compartment paired with 4-Hz light stimulation and the compartment that was not paired with light stimulation for mice expressing ChR2 or eYFP in LH_{VGLUT2} neurons. (**p < 0.01; data represent means ± SEM).

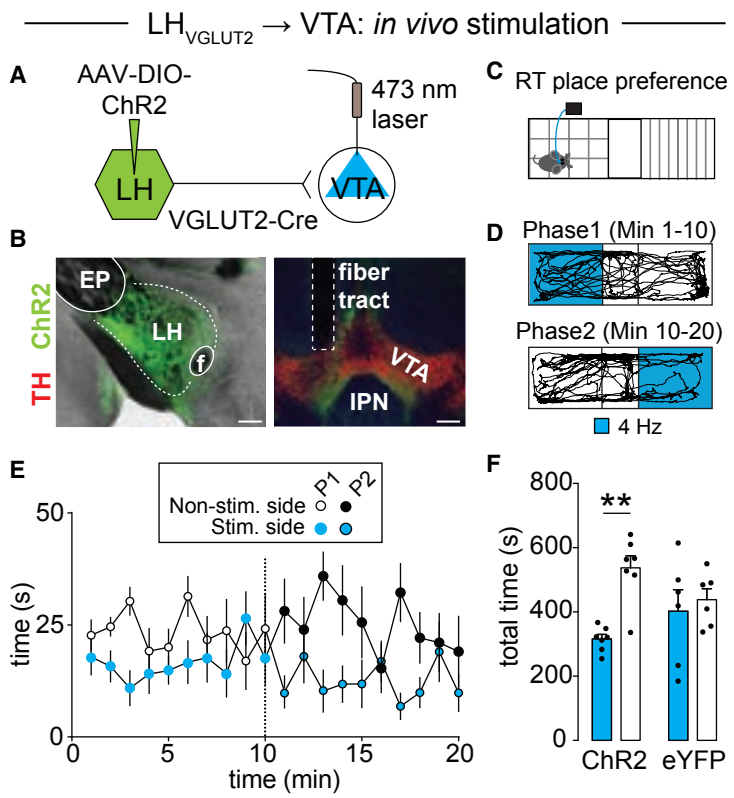

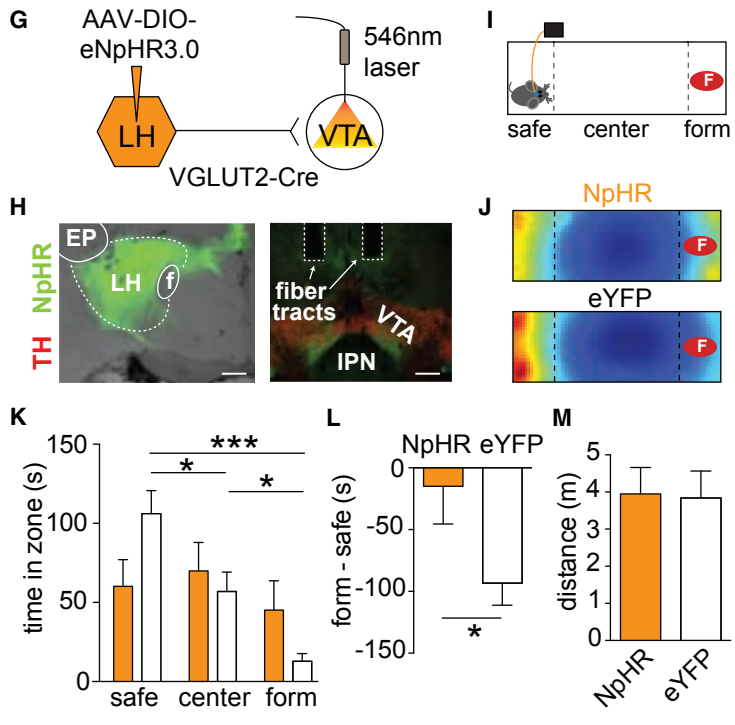

Figure 4. Bidirectional Modulation of Aversion Behavior by LH$_{VGLUT2}$ Inputs to VTA

(A) Schematic of experimental design.

(B) ChR2-eYFP (green) expression in LH neurons (left; EP, entopeduncular nucleus; f, fornix; scale bar, 250 μm) and in LH terminals in the VTA (right; red, TH; IPN, interpeduncular nucleus; scale bar, 500 μm).

(C) Schematic of real-time place preference assay.

(D) Trajectory of an animal that received 4-Hz stimulation in one compartment (phase 1 [P1], blue, top panel) for the initial 10-min period and then in the other compartment (phase 2 [P2], blue, lower panel) for an additional 10 min.

(E) Time spent in individual compartments (non-stimulated side, white; stimulated side, blue) plotted as a function of time over the course of the experiment (1-min intervals). Dashed line indicates switching of compartment stimulation after 10 min (data represent means ± SEM).

(F) Mice expressing ChR2, but not eYFP, in LH$_{VGLUT2}$ neurons spent significantly less time on the side of the chamber paired with 4-Hz optical stimulation (**$p < 0.01$; data represent means ± SEM).

(G) Schematic of experimental design.

(H) eNpHR3.0 (green) expression in LH$_{VGLUT2}$ neurons (left; scale bar, 250 μm) and in LH$_{VGLUT2}$ terminals in the VTA (right; scale bar, 500 μm).

(I) Schematic of approach-avoidance assay (F, formaldehyde, form).

(J) Heatmaps (top, NpHR; bottom: control animals) show normalized time spent in different areas of the chamber (warmer colors indicate more time spent).

(K) Mean time control (white) and NpHR (orange) mice spent in different zones (safe [i.e., greatest distance to aversive stimulus], center, form) of the chamber (*$p < 0.05$, ***$p < 0.001$; data represent means ± SEM).

(L) Mean difference scores ([time spent in form zone] – [time spent in safe compartment]) for NpHR and control (Ctrl) mice (*$p < 0.05$; data represent means ± SEM).

(M) Mean total distance traveled for NpHR and Ctrl mice ($p > 0.05$; data represent means ± SEM).

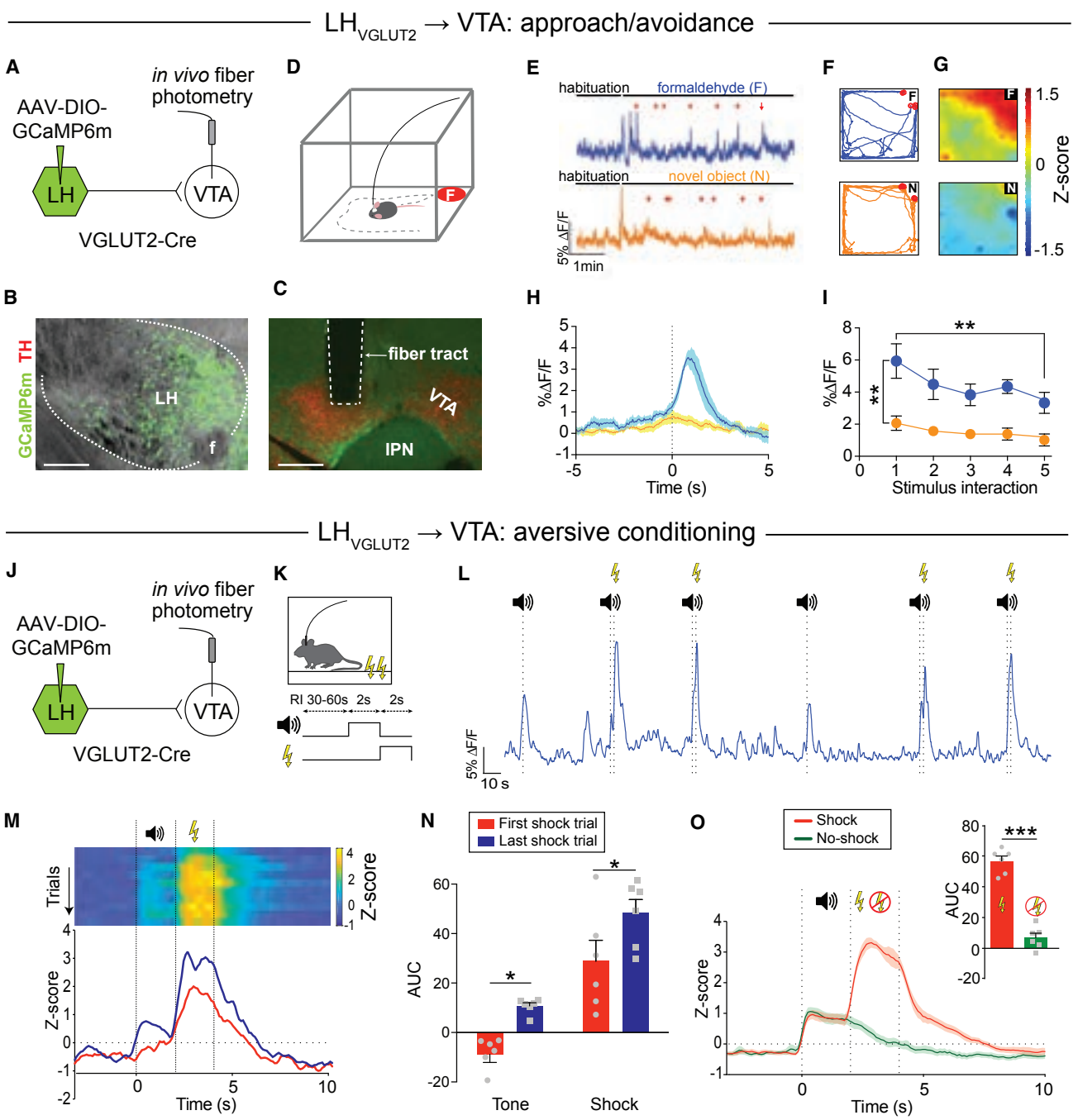

Figure 5. Activation of LH_{VGLUT2} Inputs to the VTA by Unconditioned and Conditioned Aversive Stimuli

(A) Schematic of experimental design.

(B) GCaMP6m (green) expression in LH_{VGLUT2} cell bodies (scale bar, 200 μm).

(C) Optical fiber tract location in the VTA and LH_{VGLUT2} terminals expressing GCaMP6m (green) in the mVTA (red, TH; scale bar, 500 μm).

(D) Schematic of approach-avoidance assay and fiber photometry setup (F, formaldehyde).

(E) Example responses to interaction with formaldehyde (top, blue) or to a novel object (bottom, orange). Red arrows, stimulus interaction (scale bars, 5% ΔF/F/1 min).

(F) Example trajectories for interaction with formaldehyde (F; top) or novel object (N; bottom). Red dots, stimulus interaction.

(G) Heatmaps for mean response intensity distribution in the open-field area for interaction with formaldehyde (top) or novel object (bottom; warmer colors indicate increased activity).

(H) Mean response intensity during the first five stimulus interactions (time = 0, dashed line) with formaldehyde (blue) or a novel object (orange). Area of light shading represents SEM.

(legend continued on next page)

an open-field assay (Figures S5H–S5K). It is possible that optogenetic stimulation of LH axons in the VTA results in backpropagating action potentials that activate other downstream structures via axon collaterals, such as the lateral habenula (LHb) (Stamatakis et al., 2016) or periaqueductal gray (PAG) (Li et al., 2018), which also could explain the aversive phenotype. To formally test this possibility, we performed dual retrograde tracing experiments and injected retrobeads coated with different fluorophores into either the VTA and LHb or VTA and PAG. Histological analysis revealed that only 1%–2% of retrogradely labeled LH neurons contained both fluorophores (Figure S6), suggesting that LH neurons projecting to VTA, LHb, or PAG represent largely independent projections with few if any collaterals.

Next, we probed whether *in vivo* silencing of LH_{VGLUT2} terminals in the VTA would alter the behavioral response to an aversive stimulus. We expressed an inhibitory opsin (eNpHR3.0) in LH_{VGLUT2} neurons and implanted optical fibers bilaterally above the VTA (Figures 4G, 4H, and S4B). 8 weeks later, we measured the approach-avoidance response to an aversive stimulus (formaldehyde) while inhibiting LH_{VGLUT2} terminals in the VTA with 580 nm light (Figure 4I). Formaldehyde presentation was used because it provided an unfamiliar aversive stimulus for which the degree of avoidance has previously been shown to be concentration dependent without altering general motor activity (Sorg et al., 2002). We found that eYFP mice (controls) spent significantly more time at the greatest distance to the aversive stimulus compared to NpHR mice (Figures 4J and 4K; safe: NpHR: 60.21 ± 16.85 s, control: 103.07 ± 16.45 s; center: NpHR: 69.89 ± 18.01 s, control: 59.38 ± 13.57 s; form: NpHR: 45.22 ± 18.43 s, control: 14.00 ± 5.84 s; NpHR: n = 11 mice, control: n = 13 mice; two-way ANOVA interaction $p = 0.024$, Holm-Sidak post hoc test). In contrast, NpHR mice showed a significant reduction in formaldehyde avoidance behavior compared to control mice (Figure 4L; Video S3; NpHR: −14.99 ± 30.45 s, n = 11 mice; control: −93.26 ± 17.89 s, n = 13 mice; $p < 0.05$, unpaired Student's t test), while locomotion was not affected (Figure 4M; NpHR: 3.95 ± 0.71 m, n = 11 mice, control: 3.84 ± 0.72 m, n = 13 mice, $p > 0.05$, unpaired Student's t test). Altogether, optogenetic stimulation of LH_{VGLUT2} inputs to the VTA promotes aversion and silencing these inputs reduces the aversive response to an unfamiliar aversive stimulus.

Selective Encoding of Aversive Stimuli by LH_{VGLUT2} Inputs to VTA

To investigate naturally occurring activity dynamics in response to an aversive stimulus in LH_{VGLUT2} inputs to the VTA, we expressed GCaMP6m in LH_{VGLUT2} neurons and implanted an optical fiber in the VTA (Figures 5A–5C and S4C). We then used fiber photometry to record calcium activity dynamics in LH_{VGLUT2} terminals in the VTA during an approach-avoidance task (Figure 5D). We observed large increases in activity that were time locked specifically to interaction with formaldehyde, but not to interaction with a novel object (Figures 5E–5H and Video S4). Quantification of the %ΔF/F for individual stimulus interactions showed significantly greater responses for formaldehyde compared to novel object interaction (Figure 5I; $p < 0.01$; two-way RM ANOVA). We also observed that the response intensity decreased significantly between the first and fifth formaldehyde interaction (Figure 5I; stimulus #1: 5.94 ± 1.08, stimulus #5: 3.51 ± 0.65, n = 6 mice; $p < 0.01$, Holm-Sidak post hoc test). Furthermore, we found that mice that interacted with formaldehyde expressed 2 times the level of the activity-dependent immediate-early gene *fos* in the LH compared to mice that interacted with a novel object, and this increase was specifically due to an increase in *fos* expression in VTA-projecting LH_{VGLUT2} neurons (Figure S7).

To examine whether this pathway plays a role in learning about aversive outcomes, we subjected another cohort of mice to the same aversive conditioning paradigm used earlier (Figures 5J and 5K). As expected, an US caused a strong increase in LH_{VGLUT2} terminal activity in the VTA. After conditioning, however, we observed a significant increase in activity in response to a CS, while the response to the shock also grew in magnitude (Figures 5L–5N; tone, first: −8.84 ± 3.29, last: 10.75 ± 1.25, shock, first: 28.86 ± 8.43, last: 48.38 ± 5.4, n = 6 mice, two-way RM ANOVA p(trial) = 0.032, tone first versus last: $p = 0.025$, shock first versus last: $p = 0.025$, Holm-Sidak post hoc test). Notably, neural activity dynamics in response to shock omission largely resembled those in vNAcMed-projecting DA terminals under the same experimental conditions (i.e., a slow but steady decrease in activity following the tone; Figure 5O; shock: 55.95 ± 3.24, no-shock: 6.44 ± 2.94, n = 6 mice, $p < 0.001$, paired Student's t test). These results raise the possibility that the increased activity dynamics in vNAcMed DA terminals in response to US and CS aversive stimuli (Figures 1G–1I) may involve direct synaptic input from LH_{VGLUT2} neurons.

Connectivity of Glutamatergic LH Neurons with VTA Subpopulations

The LH is a major source of monosynaptic input to VTA DA neurons (Figure 3D) (Beier et al., 2015), but functional investigations

(I) %ΔF/F for individual stimulus interactions shows significantly greater responses for formaldehyde compared with novel object interaction. Note that the response intensity decreases significantly between first and fifth formaldehyde interaction (**$p < 0.01$; data represent means ± SEM).
(J) Schematic of experimental design.
(K) Schematic of aversive conditioning paradigm.
(L) Representative sample of LH_{VGLUT2} terminal activity in response to tone and foot shock. Note that both the "tone-shock" trials and "tone-only" (omission) trials increase activity in LH_{VGLUT2} terminals in the VTA (recorded during the omission session, i.e., 24 hr after conditioning).
(M) Top: representative heatmaps showing the individual *Z* scores for trials in which a 2-s tone was followed by a 2-s electrical foot shock (ordered from first to last shock trial). Bottom: example responses to the tone and foot shock in an unconditioned animal (first shock trial, red) and after conditioning (last shock trial, blue).
(N) Mean AUC during tone and shock before (red) and after (blue) aversive conditioning (*$p < 0.05$; data represent means ± SEM).
(O) Comparison of *Z* score averages for trials in which a tone was followed by a foot shock (red) or was omitted (green; 67% foot shock probability). Inset shows significantly increased activity (quantified as AUC) in omission (no shock) compared with shock trials (***$p < 0.001$; data represent means ± SEM).

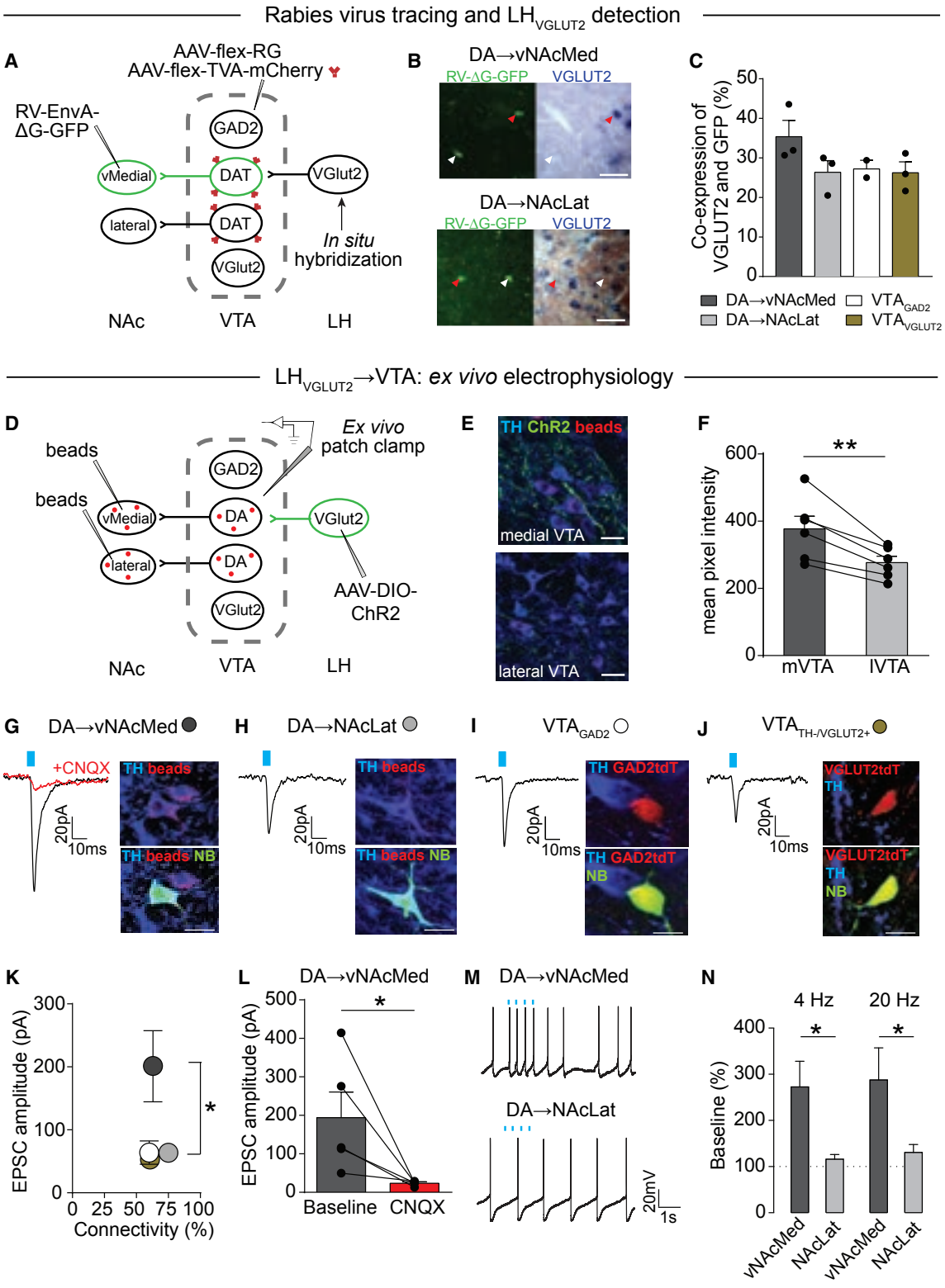

Figure 6. LH$_{VGLUT2}$ Neurons Preferentially Target and Activate vNAcMed-Projecting DA Neurons

(A) Schematic of experimental design to analyze VGLUT2 mRNA expression in LH neurons synapsing on vNAcMed-projecting DA neurons in DAT-Cre mice. VGLUT2-Cre and GAD2-Cre mice were used to determine connectivity of glutamatergic and GABAergic VTA neurons with LH$_{VGLUT2}$ neurons.

(legend continued on next page)

have suggested that LH_{VGLUT2} neurons also modulate the activity of non-DA VTA neurons (Nieh et al., 2016). To explore whether differences may exist in the synaptic connectivity of LH_{VGLUT2} neurons with different VTA cell types, we combined *in situ* hybridization with *trans*-synaptic rabies tracing (Figure 6A). Rabies tracing of genetically identified VTA GABA and glutamate neurons (VTA_{GAD2} and VTA_{VGLUT2}, respectively), as well as vNAcMed- and NAcLat-projecting DA neurons, produced labeling of presynaptic neurons in the LH. VGLUT2 mRNA was detected in ~26%–36% of LH input neurons with no major quantitative differences between VTA cell populations (Figures 6B and 6C; Table S1B; vNAcMed: 35.38 ± 4.10%, n = 3 mice; NAcLat: 26.36 ± 2.95%, n = 3 mice; VTA_{GAD2}: 27.21 ± 2.21%, n = 2 mice; VTA_{VGLUT2}: 26.25 ± 2.75%, n = 3 mice).

To examine functional connectivity, we made whole-cell recordings from vNAcMed- and NAcLat-projecting DA neurons as well as genetically identified VTA GABA and glutamate neurons (Figure 6D). Notably, LH_{VGLUT2} terminals were predominantly located in the mVTA adjacent to vNAcMed-projecting DA neurons (Figures 6E and 6F; mVTA: 377.4 ± 37.54, lVTA: 277.0 ± 18.60, n = 6 mice, $p < 0.01$, paired Student's t test), hinting at possible differences in synaptic connectivity compared with DR_{VGLUT3} inputs, which were located in the lVTA and activated NAcLat-projecting DA neurons (Figures 3E–3L). Although optical stimulation of LH terminals generated EPSCs in all VTA cell populations with a similar response rate (~60%–75%), light-evoked EPSCs were on average 3-fold larger in vNAcMed-projecting DA neurons (Figures 6G–6K; vNAcMed: 199.5 ± 55.28 pA, n = 21/32 cells (65.6%); NAcLat: 63.71 ± 14.06 pA, n = 15/20 cells (75%), 19 mice; GAD2: 63.93 ± 18.53 pA, n = 9/15 cells (60%), 3 mice; VGLUT2: 52.79 ± 12.98 pA, n = 20/33 cells (60.6%), 4 mice; $p < 0.05$, Mann-Whitney test). These EPSCs were blocked by 10 μM CNQX, indicating that LH terminals released glutamate (Figure 6L; baseline: 193.9 ± 66.54 pA, CNQX: 23.51 ± 2.72 pA, n = 5 cells, $p < 0.05$, paired Student's t test). Importantly, vNAcMed- but not NAcLat-projecting DA neurons, recorded in the same set of slices, increased firing in response to both 4- and 20-Hz optical stimulation of LH_{VGLUT2} inputs (Figures 6M and 6N; 4 Hz: vNAcMed: 250.3 ± 52.17%, n = 7 cells, NAcLat: 115.9 ± 10.35%, n = 9 cells; 20 Hz: vNAcMed: 287.4 ± 69.8%, n = 8 cells, NAcLat: 130.6 ± 17.35%, n = 7 cells, 9 mice; two-way ANOVA p(projection) = 0.003, Holm-Sidak post hoc $p < 0.05$ for both projections). Thus, stimulation of LH_{VGLUT2}-expressing terminals did not change the firing frequency of the NAcLat-projecting population, despite evidence that LH_{VGLUT2} neurons make synaptic connections onto VTA GABA cells (Figure 6I), which theoretically could lead to an inhibition of VTA DA neurons (Nieh et al., 2016). Taken together, although LH_{VGLUT2} neurons target several VTA cell populations, vNAcMed-projecting DA neurons represent a major downstream target.

LH_{VGLUT2} Neurons Activate vNAcMed-Projecting DA Neurons to Regulate Aversive Behaviors

Inhibition of VTA DA neurons via local GABA neurons contributes to aversion-related behavior (Tan et al., 2012). Consistent with this notion is our finding that NAcLat DA terminals are depressed in response to aversive stimuli (Figures 1D–1F). However, the surprising finding that stimulation of LH_{VGLUT2} terminals does not result in an inhibition of NAcLat-projecting DA neurons (Figures 6M and 6N) raises the possibility that the aversion phenotype we observed in response to optogenetic stimulation of LH_{VGLUT2} inputs (Figures 4A–4F) may primarily result from an excitation of vNAcMed-projecting DA neurons rather than indirect inhibition of NAcLat-projection DA neurons. To examine synaptic connectivity *in vivo*, we combined optogenetic stimulation of LH_{VGLUT2} inputs to the VTA with fiber photometry of VTA terminals in the vNAcMed or NAcLat. We injected VGLUT2-Cre mice with AAV-DIO-ChR2-mCherry into the LH and AAV-Syn-GCaMP6m into the VTA and implanted two optical fibers—one in the VTA and the other in either vNAcMed or NAcLat. This enabled us to shine blue light over the VTA to activate LH_{VGLUT2} terminals while simultaneously recording VTA terminal activity in the vNAcMed or NAcLat. A limitation of this approach is that we recorded from both DA and non-DA terminals, though previous work has suggested that the majority of NAcLat- and NAcMed-projecting VTA neurons are DAergic (Lammel et al., 2011). We found that activation of LH_{VGLUT2} inputs with 20-Hz stimulation

(B) Sample images showing VGLUT2-positive (red arrow) and VGLUT2-negative (white arrow) LH neurons (GFP-positive, green) that make monosynaptic connections onto vNAcMed- (top) or NAcLat-projecting DA neurons (bottom; scale bars, 20 μm).
(C) Mean percentage of presynaptic VGLUT2-expressing LH neurons for different VTA cell populations (data represent means ± SEM).
(D) Schematic of experimental design.
(E) ChR2-eYFP expressing glutamatergic LH terminals (green) are more frequently in the mVTA adjacent to retrogradely labeled (beads, red) TH-immunopositive (blue) cells projecting to vNAcMed (top) than in the lVTA (bottom; scale bars, 10 μm).
(F) Mean fluorescence intensity (analyzed as mean pixel intensity) of ChR2-eYFP expression in LH terminals in the mVTA compared with lVTA (**$p < 0.01$; data represent means ± SEM).
(G–J) EPSCs generated by stimulation of LH inputs in retrogradely labeled (beads, red) VTA neurons projecting to (G) vNAcMed (red trace: after CNQX application) or (H) NAcLat and in VTA neurons expressing (I) GAD2 (tdTomato-positive, red) or (J) VGLUT2 (tdTomato-positive, red). Cells were filled with neurobiotin (NB, green) and are TH immunopositive (blue) for (G) and (H) and TH immunonegative for (I), (J; scale bars: 20 pA/10 ms; 10 μm).
(K) Mean EPSCs amplitudes and response probabilities generated by stimulation of LH inputs in 4 VTA cell populations (same color code as in G–J; *$p < 0.05$; data represent means ± SEM).
(L) Mean EPSC amplitudes recorded in vNAcMed-projecting DA neurons before (gray) and after (red) bath application of 10 μM CNQX (*$p < 0.05$; data represent means ± SEM).
(M) Spontaneous firing in vNAcMed- (top) and NAcLat-projecting (bottom) DA neurons and 4-Hz stimulation of LH_{VGLUT2} terminals (recorded in the same slice; scale bar, 20 mV/1 s).
(N) Relative increase in firing rate during 4- and 20-Hz LH_{VGLUT2} terminal stimulation for vNAcMed- and NAcLat-projecting DA neurons (*$p < 0.05$; data represent means ± SEM).

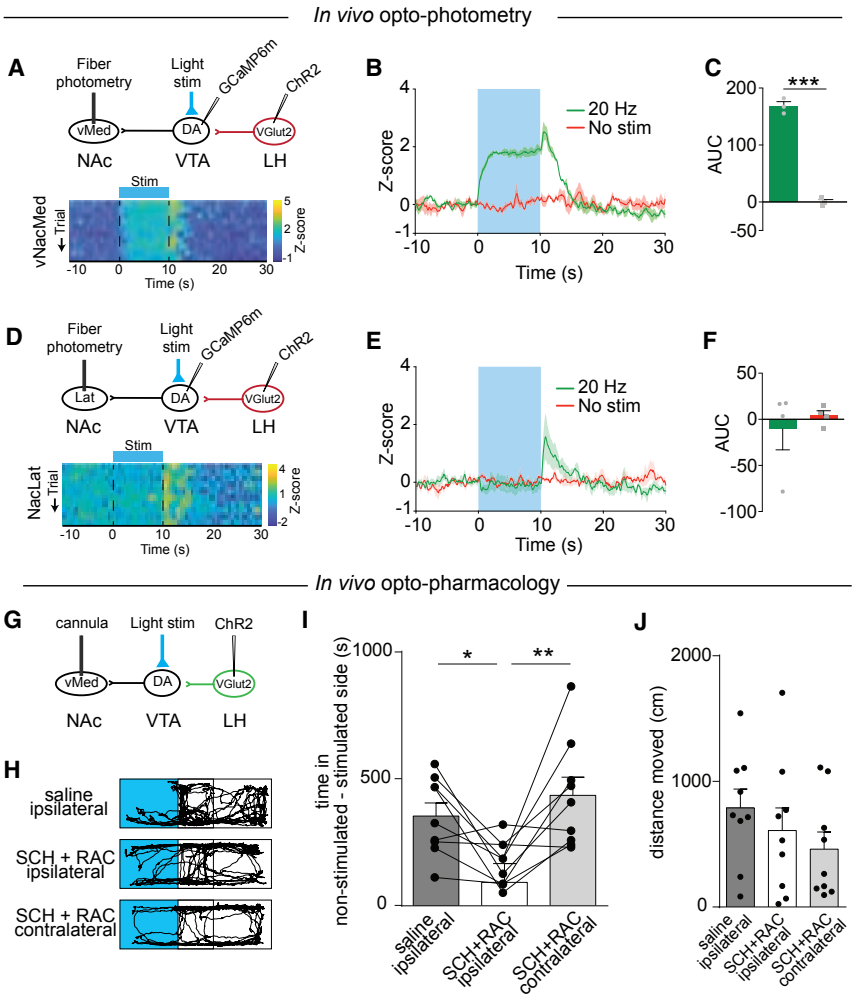

Figure 7. LH_{VGLUT2} Neurons Activate vNAcMed-Projecting DA Neurons to Regulate Aversive Behaviors

(A) Top: schematic of experimental design. Bottom: representative heatmaps of individual *Z* scores during stimulation trials.

(B) *Z* score averages of stimulation (green) and no-stimulation (red) trials (data represent means ± SEM).

(C) Mean AUC in the vNAcMed during stimulation (green) and no stimulation (red; ***$p < 0.001$; data represent means ± SEM).

(D) Top: schematic of experimental design. Bottom: representative heatmaps of individual *Z* scores during stimulation trials.

(E) *Z* score averages of stimulation (green) and no-stimulation (red) trials (data represent means ± SEM).

(F) Mean AUC in the NAcLat during stimulation (green) and no stimulation (red; data represent means ± SEM).(G) Schematic of experimental design, which involves infusion of D1 (SCH23390 [SCH]) and D2 (raclopride [RAC]) receptor antagonists in to the vNAcMed and optogenetic stimulation of LH_{VGLUT2} terminals in the VTA.

(H) Trajectories of animals that received SCH and RAC infusion into the vNAcMed and LH_{VGLUT2} terminal stimulation in VTA.

(I) Mean time spent in non-stimulated minus stimulated side for different experimental conditions (one data point outside axis limits; *$p < 0.05$, **$p < 0.01$; data represent means ± SEM).

(J) Mean total distance animals traveled during the experiment (data represent means ± SEM).

significantly increased emitted fluorescence signals in the vNAcMed, compared to fluorescence signals without optogenetic stimulation (Figures 7A–7C; 20 Hz: 168.3 ± 7.75, no stim: 0.15 ± 4.08, n = 3 mice, p = 0.002, paired Student's t test). In contrast, when we stimulated LH_{VGLUT2} inputs and recorded in the NAcLat, we only observed a small decrease in emitted fluorescence signals, which was not significantly different from fluorescence in the absence of stimulation (Figures 7D–7F; 20 Hz: −10.14 ± 22.94, no stim: 4.17 ± 5.16, n = 4 mice, p = 0.49, paired Student's t test). It is unlikely that the lack of inhibition in the NAcLat is due to methodological issues since we verified all optical fiber placements and also observed a robust increase in fluorescence intensity immediately after optogenetic stimulation in both NAcLat and vNAcMed. Though also noticed by others (Nieh et al., 2016), the meaning of this rebound excitation remains unknown.

To test whether DA receptor activation in the vNAcMed is required for aversive behavior induced by optogenetic stimulation of LH_{VGLUT2} terminals in the VTA, we expressed ChR2 unilaterally in LH_{VGLUT2} neurons and implanted an optical fiber dorsal to the VTA and infusion cannulas bilaterally in the vNAcMed (Figure 7G). We then optogenetically stimulated LH_{VGLUT2} inputs in the VTA during a real-time place preference assay 5 min after infusing either saline or D1 and D2 receptor antagonists (30 ng SCH23390 [SCH] and 300 ng raclopride [RAC], respectively; dissolved in 0.3 μL saline) into the ipsilateral or contralateral vNAcMed. While ipsilateral infusion of saline or contralateral infusion of SCH and RAC resulted in immediate place avoidance behavior during stimulation of LH_{VGLUT2} terminals in the VTA, as observed previously in the absence of DA receptor antagonism (Figures 4A–4F), ipsilateral infusion of SCH and RAC significantly reduced place avoidance behavior (Figures 7H and 7I; saline: 353.2 ± 50.99 s; SCH+RAC ipsilateral: 91.55 ± 73.59 s; SCH+RAC contralateral: 434.8 ± 71.25 s, n = 9 mice, one-way RM ANOVA, p = 0.001, saline versus ipsilateral p = 0.024, ipsilateral versus contralateral p = 0.006, Tukey's post hoc test). It is unlikely that the reduction in place aversion is caused by a general decrease in locomotor activity, as statistical comparison of the total distance traveled did not yield any significant differences for the 3 groups (Figure 7J; saline: 609.9. ± 180 cm; SCH+RAC ipsilateral: 789.9 ± 148.6 cm; SCH+RAC contralateral: 461.6 ± 135.1 cm, n = 9 mice, two-way RM ANOVA, p = 0.11). Taken together, our data suggest that a subtype of mesolimbic DA neurons may represent a critical link in the transfer of aversive information from LH_{VGLUT2} neurons to the vNAcMed.

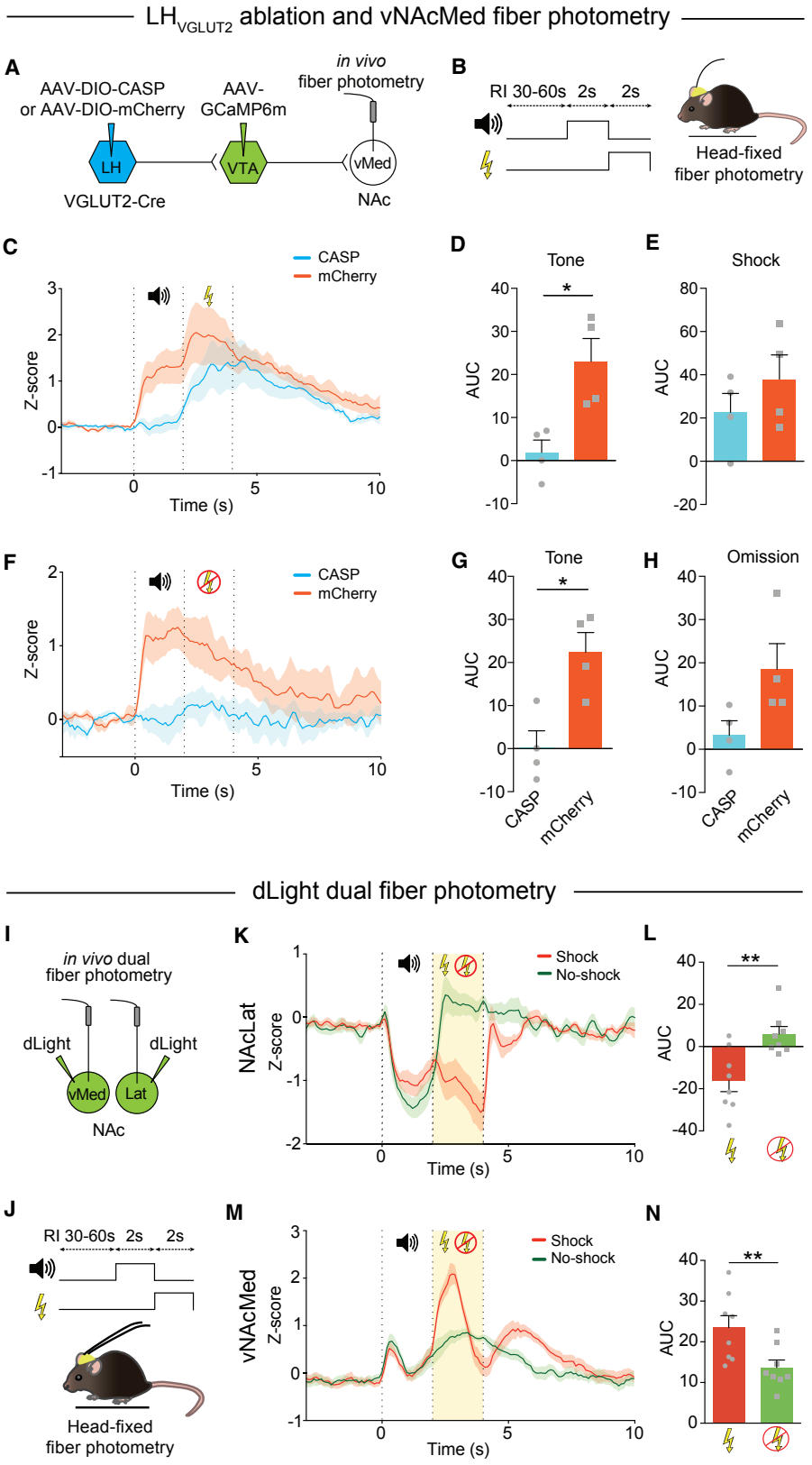

(legend on next page)

LH_{VGLUT2} Inputs Are Necessary for the Encoding of Aversive-Predicting Stimuli in vNAcMed-Projecting DA Neurons

Both VTA terminals that originate from LH_{VGLUT2} neurons and DA terminals in the vNAcMed are activated by aversive stimuli and cues that predicted them (Figures 1 and 5). To test whether LH_{VGLUT2} neurons are necessary components for the encoding of unconditioned and/or conditioned aversive stimuli in the mesolimbic system, we sought to selectively ablate LH_{VGLUT2} neurons. To do this, we induced apoptosis selectively in these cells by infusing a Cre-dependent AAV expressing Caspase 3 (Yang et al., 2013) in the LH of VGLUT2-Cre mice (CASP, n = 4 mice). In the same animals, AAV-Syn-GCaMP6m was infused into the VTA, and an optical fiber was implanted in the vNAcMed. Control animals received injections of AAV-DIO-mCherry in the LH, while all other procedures were identical (mCherry, n = 4 mice) (Figure 8A). 5 weeks later, animals were subjected to an aversive conditioning procedure while performing fiber photometry recordings from vNAcMed terminals with their head fixed in place (Figure 8B). In control mice, consistent with our previous findings (Figure 1H), we observed increased activity patterns in vNAcMed terminals in response to an aversive US (which decreased in subsequent trials), while activity patterns to CS were significantly increased only after conditioning. Strikingly, while activity dynamics to the US remained largely unaffected in CASP mice, ablation of LH_{VGLUT2} neurons prevented the excitatory response to CS in both shock (Figures 8C–8E and S8; tone: CASP: 1.89 ± 2.89, n = 4 mice, mCherry: 23 ± 4.35, n = 4 mice, p = 0.013 unpaired Student's t test; shock: CASP: 22.6 ± 8.76, n = 4, mCherry: 37.98 ± 11.26, n = 4, p = 0.32, unpaired Student's t test) and shock omission trials (Figures 8F–8H; tone: CASP: 0.1 ± 3.8, n = 4 mice, mCherry: 21.51 ± 4.46, n = 4 mice, p = 0.011 unpaired Student's t test; omission: CASP: 3.25 ± 3.36, n = 4, mCherry: 18.53 ± 5.91, n = 4, p = 0.066, unpaired Student's t test).

VTA DA neurons may co-release glutamate in the NAc (Stuber et al., 2010) and VGLUT2 is preferentially co-expressed in NAcMed-projecting DA neurons (Yang et al., 2018). It is possible that the excitatory responses to aversive stimuli in our GCaMP6m-based fiber photometry experiments may involve functionally and chemically heterogeneous inputs to the vNAcMed. To achieve highly specific optical readout of changes in DA transients in response to US and CS aversive stimuli, we used an intensity-based genetically encoded DA indicator (dLight1.1), which is specific to DA and does not respond to glutamate and GABA (Patriarchi et al., 2018). We infused dLight1.1 into the vNAcMed and NAcLat of C57Bl6 mice (n = 8 mice) and implanted optical fibers in these regions (Figure 8I). Head-fixed animals were subjected to the aversive conditioning procedure and DA transients were imaged simultaneously using dual fiber photometry (Figure 8J). Our recordings in the NAcLat revealed decreased DA responses to US and CS and increased DA transients in response to omission of a predicted shock (Figures 8K and 8L; shock: −15.99 ± 5.17, no-shock: 6.06 ± 3.56, n = 8 mice, p = 0.002, paired Student's t test). Conversely, DA responses in the vNAcMed were increased to the US and CS but were significantly reduced when a predicted shock was omitted (Figures 8M and 8N; shock: 23.51 ± 2.96, no-shock: 13.66 ± 1.86, n = 8 mice, p = 0.004, paired Student's t test). Together, these results demonstrate that the encoding of aversive outcomes involves both LH_{VGLUT2} neurons and increased DA transients in the vNAcMed.

DISCUSSION

Here, we provide a detailed dissection of the neural circuit architecture of the mesolimbic DA system during appetitive and aversive behaviors. A striking result is the functional topography of DA signaling in the NAc, with aversive prediction signaling predominantly restricted to the vNAcMed and reward prediction signaling in the NAcLat. Furthermore, we demonstrate that LH_{VGLUT2} neurons represent a key input for providing information about aversive outcomes to vNAcMed-projecting DA neurons.

Heterogeneity in the Mesolimbic DA System

The mesolimbic DA system has long been hypothesized to play a major role in both reward and aversive processing, yet defining these dual functions has been a challenge. Different techniques and model organisms have sometimes yielded opposing narratives that are difficult to explain. For example, human imaging studies have pointed to the co-existence of both appetitive and aversive signals within the NAc (Baliki et al., 2010; Delgado et al., 2008, 2011; Seymour et al., 2007), and numerous fast-scan

Figure 8. Encoding of Future Aversive Outcomes Involves LH_{VGLUT2} Neurons and Increased Dopamine Transients in the vNAcMed

(A) Schematic of experimental design.

(B) Schematic of aversive conditioning paradigm in head-fixed mice.

(C) Comparison of *Z* score averages for trials in which a tone was followed by a foot shock for mice expressing CASP (blue) or mCherry (red) in LH_{VGLUT2} neurons.

(D and E) Mean AUC during tone (D) and shock (E) after aversive conditioning for mice expressing CASP and mCherry in LH_{VGLUT2} neurons (*p < 0.05; data represent means ± SEM).

(F) Comparison of *Z* score averages for trials in which the foot shock was omitted for mice expressing CASP (blue) or mCherry (red) in LH_{VGLUT2} neurons.

(G and H) Mean AUC during tone (G) and shock omission (H) after aversive conditioning for mice expressing CASP or mCherry in LH_{VGLUT2} neurons (*p < 0.05; data represent means ± SEM). (I) Schematic of experimental design.

(J) Schematic of aversive conditioning paradigm in head-fixed mice and fiber photometry of DA transients in the vNAcMed and NAcLat.

(K) Comparison of *Z* score averages for DA transients in the NAcLat for trials in which a tone was followed by a foot shock (red) or was omitted (green; 67% foot shock probability).

(L) AUC during shock delivery versus shock omission (no-shock trials) for DA transients in the NAcLat (**p < 0.01; data represent means ± SEM).

(M) Comparison of *Z* score averages for DA transients in the vNAcMed for trials in which a tone was followed by a foot shock (red) or was omitted (green; 67%-foot shock probability).

(N) AUC during shock delivery versus shock omission (no-shock trials) for DA transients in the vNAcMed (**p < 0.01; data represent means ± SEM).

voltammetry and microdialysis studies have shown that aversive stimuli can increase DA release in several NAc subregions (Abercrombie et al., 1989; Anstrom et al., 2009; Badrinarayan et al., 2012; Bassareo et al., 2002; Budygin et al., 2012; Deutch and Cameron, 1992; Martinez et al., 2008; Young, 2004). In contrast, an extensive and important body of work based mainly on single-unit recordings in awake behaving primates has demonstrated that VTA DA neurons show characteristic phasic responses to rewards and cues that predict them and are inhibited by aversive events (Fiorillo, 2013; Mirenowicz and Schultz, 1996; Schultz, 2016; Stauffer et al., 2016; Ungless et al., 2004; Watabe-Uchida et al., 2017).

Recent hypotheses, however, have attempted to merge and justify the opposing narratives by suggesting that anatomically and functionally distinct midbrain DA neuron subtypes may encode different signals and participate in largely separate circuits (Bromberg-Martin et al., 2010; Lammel et al., 2014; Lerner et al., 2016; Menegas et al., 2017; Morales and Margolis, 2017). Still, compelling arguments have been made that some excitatory responses to aversive events may be due to high-reward contexts, physical impact, or to the rewarding effects of terminating the aversive stimulus (Fiorillo, 2013; Schultz, 2016; Seymour et al., 2005; Tanimoto et al., 2004). By simultaneously recording DA terminal activity in different NAc subregions, we directly tested whether distinct mesolimbic DA subtypes exclusively signal aspects of reward or aversion or whether they serve a broader function of signaling salience regardless of value. We found that both aversive-predictive cues and unpredicted foot shock produced a transient increase in DA terminal activity selectively in the vNAcMed, while activity was persistently depressed in all other NAc subregions. Such anatomical specificity is consistent with a recent fast-scan cyclic voltammetry study in which responses to a fear-evoking cue resulted in decreased DA transmission within the NAc core but increased transmission within the NAc medial shell, although on a different timescale (Badrinarayan et al., 2012). Importantly, we demonstrate that conditioned and unconditioned aversive stimuli elicit distinct responses in NAcMed DA terminals along the dorso-ventral axis, suggesting a functional anatomical segregation of DA signaling even within the NAcMed. These differences could explain why several studies have reported opposite effects on DA release measured in response to aversive stimuli in the same NAc subregion (McCutcheon et al., 2012). Moreover, our finding that anatomically distinct NAcMed subregions promote opposite motivational states is consistent with the notion that liking, or pleasure itself, is generated through the activation of kappa opioid receptor in small, "hedonic hotspots" within the rostrodorsal region of the NAcMed (Berridge and Kringelbach, 2015; Peciña and Berridge, 2005), whereas selective activation of cells expressing these receptors in the ventral region of the NAcMed promotes behavioral aversion (Al-Hasani et al., 2015).

A Unique Mesolimbic DA Subtype for Aversive Learning

The striking finding that vNAcMed DA terminals are activated in response to conditioned and unconditioned aversive stimuli still leaves unanswered the question of what type of information these cells encode. Do these cells encode motivational salience as it has been proposed for DA neurons in the lateral SNc (Lerner et al., 2015; Matsumoto and Hikosaka, 2009; Menegas et al., 2017)? vNAcMed DA terminals signal information about the cessation of an aversive stimulus as indicated by the rebound excitation at the offset of the aversive stimulus, although it remains unclear whether this signal could be interpreted as a relief or safety signal (Budygin et al., 2012; Lloyd and Dayan, 2016; Seymour et al., 2005). After reward conditioning, excitation to reward-predicting cues dominates in NAcLat DA terminals, which is consistent with the idea that lVTA DA neurons are remarkably homogeneous in regard to reward prediction error coding (Eshel et al., 2016). Although reward omission did not lead to a decrease in neural activity in NAcLat DA terminals, it has been generally difficult to unequivocally identify negative prediction signals in well-trained animals (Watabe-Uchida et al., 2017). Importantly, while vNAcMed DA terminals initially showed a robust excitation to reward delivery, we could not detect a response to reward-predicting cues, even after extensive training. Nevertheless, there was an increase in activity during reward anticipation (Figures 2L and S2B), which is reminiscent of the elevated DA release during self-initiated reward consumption (Roitman et al., 2004; Wassum et al., 2012) and might reflect the initiation of an action (e.g., tongue protrusion during consumption of sucrose reward).

Despite the striking differences in vNAcMed and NAcLat DA terminals, a limitation of our fiber photometry approach is that there is little information about how uniform the activity is across neurons. We cannot exclude the possibility that the changes in net activity we observed is just the dominant pattern of activity in a small subset of neurons. However, given that all recordings were performed in the same animals and under the same experimental conditions, our data strongly suggest substantial differences in aversive and appetitive learning for distinct mesolimbic DA subtypes.

Afferent Control in the Mesolimbic DA System

VTA DA neurons receive synaptic input from numerous brain regions (Beier et al., 2015), but the mechanisms by which these cells integrate information about motivational stimuli remain largely unknown. The LHb is a major input to the VTA-RMTg, and LHb neurons are excited in response to aversive stimuli (Matsumoto and Hikosaka, 2007). However, LHb neurons do not make functional synaptic connections onto mesolimbic DA neurons but instead target mesocortical DA neurons and RMTg GABA neurons (Jhou et al., 2009; Lammel et al., 2012). If LHb neurons do not directly excite mesolimbic DA neurons, what other inputs to the VTA might be responsible for directly driving downstream excitation in response to aversive stimuli? Even though anatomically the DR provides strong input to vNAcMed-projecting DA neurons, we found that on a functional level—at least for glutamatergic input—NAcLat-projecting DA neurons represent a major downstream target. It is noteworthy, however, that the DR contains heterogeneous cell populations compromising serotonergic, glutamatergic, and GABAergic neurons, and co-release of these neurotransmitters has been reported (Liu et al., 2014; McDevitt et al., 2014). Thus, although our results suggest that it is unlikely that glutamatergic DR input

contributes to the increased activity of vNAcMed-projecting DA neurons in response to aversive stimuli, we cannot exclude the possibility that DR serotonin or GABA transmission influences the encoding of aversive stimuli in these cells.

On the other hand, we found that LH_{VGLUT2} neurons both anatomically and functionally constitute a dominant presynaptic input to vNAcMed-projecting DA neurons. LH_{VGLUT2} neurons may also di-synaptically inhibit DA neurons in the lVTA indirectly via local GABA neurons, and as a result decrease DA levels in the NAc (Nieh et al., 2016). Although we did not observe a decrease in activity in response to LH_{VGLUT2} input stimulation in NAcLat-projecting DA neurons in our *ex vivo* slice preparation (Figures 5M and 5N), and our opto-fiberphotometry experiments did not show decreased activity in the NAcLat (Figures 7D–7F), we cannot exclude the possibility that a fraction of DA neurons projecting to the NAcLat (or other NAc subregions) may be part of a di-synaptic inhibitory circuit. Thus, despite the fact that both LH_{VGLUT2} and LHb inputs to the VTA promote aversion, there are important differences in the functional connectivity with VTA DA subpopulations. We speculate that di-synaptic inhibition of NAcLat-projecting DA neurons through LHb neurons may be critical for the inhibition of these cells in response to aversive stimuli and/or during reward omission (Tian and Uchida, 2015). Conversely, after ablation of LH_{VGLUT2} neurons, we observed that vNAcMed terminals maintained their excitatory responses to unpredicted aversive stimuli (although there was some reduction), while they completely lost their ability to respond to aversive-predicting stimuli. Thus, LH_{VGLUT2} neurons are likely not the only source, and other inputs may determine the excitation of vNAcMed DA terminals in response to unpredicted aversive stimuli. Moreover, we do not expect that LH_{VGLUT2} neurons exclusively influence vNAcMed-projecting DA neurons since they also synapse onto other VTA subpopulations (e.g., glutamatergic neurons), and there are notable differences in the calcium dynamics between vNAcMed DA and LH_{VGLUT2} terminals (e.g., LH_{VGLUT2} terminals lack a rebound excitation at shock offset).

In support of traditional computational models (Daw et al., 2006; Doya, 2008), we provide empirical evidence that separate inputs to VTA DA neurons serve a specific function. Accordingly, LH_{VGLUT2} neurons are necessary for determining excitation specifically to aversive-predicting cues in a subtype of VTA DA neurons, which may facilitate learning about aversive outcomes. This does not exclude the possibility, however, that discrete brain regions may simultaneously encode partial attributes about these stimuli, which then converge onto separate groups of DA cells that integrate this information in order to respond to environmental stimuli (Tian et al., 2016). For example, encoding stimulus attributes for reward prediction error may be redundant or partially computed in the prefrontal cortex (PFC) (Starkweather et al., 2018), laterodorsal tegmental nucleus (LDT) (Lammel et al., 2012), and DR (Figure 3; (Liu et al., 2014; McDevitt et al., 2014; Qi et al., 2014) and transmitted to NAcLat-projecting DA neurons, while LH (Figures 4 and 5) (Nieh et al., 2016) and bed nucleus of the stria terminalis (BNST) (Jennings et al., 2013) may carry information to vNAcMed-projecting DA neurons contributing to aversive learning.

STAR★METHODS

Detailed methods are provided in the online version of this paper and include the following:

- KEY RESOURCES TABLE
- CONTACT FOR REAGENT AND RESOURCE SHARING
- EXPERIMENTAL MODEL AND SUBJECT DETAILS
- METHOD DETAILS
  - Stereotaxic surgeries
  - Electrophysiology
- OPTOGENETICS AND BEHAVIORAL ASSAYS
  - Aversive Conditioning
  - Reward Conditioning
  - Real-time Place Preference
  - Open Field Test
  - Approach-Avoidance Task
  - Opto-pharmacology
- FIBER PHOTOMETRY
- RABIES VIRUS TRACING
- *IN SITU* HYBRIDIZATION
- HISTOLOGY AND MICROSCOPY
- QUANTIFICATION AND STATISTICAL ANALYSIS

SUPPLEMENTAL INFORMATION

Supplemental Information includes eight figures, one table, and four videos and can be found with this article online at https://doi.org/10.1016/j.neuron.2018.11.005.

A video abstract is available at https://doi.org/10.1016/j.neuron.2018.11.005#mmc7.

ACKNOWLEDGMENTS

We thank the UNC vector core for AAV viruses and the UC Berkeley CNR Biological Imaging Facility. S.L. is a John P. Stock Faculty Fellow and Rita Allen Scholar. This work was supported by an NIH grant (R01-DA042889), a NARSAD Young Investigator Award (23543), a Brain Research Foundation grant (BRFSG-2015-7), and the Wayne and Gladys Valley Foundation. K.D. is supported by NIMH and NIDA. I.P.D. is supported by a postdoctoral fellowship from the Wenner-Gren Foundations.

AUTHOR CONTRIBUTIONS

Stereotactic Injections, J.J. and S.A.A.; Immunohistochemistry, J.J., J.R.P., C.L., and S.A.A.; Electrophysiology, J.J.; Behavior, J.J. and S.A.A.; Fiber Photometry, J.J. and I.P.D.; Training for Fiber Photometry and Critical Reagents, L.T., C.K.K., and K.D.; Study Design, Analysis, and Interpretation, J.J., S.A.A., and S.L.; Manuscript – Writing, J.J. and S.L.; Manuscript – Editing, all authors.

DECLARATION OF INTERESTS

The authors declare no competing interests.

Received: June 19, 2018
Revised: October 4, 2018
Accepted: November 2, 2018
Published: November 29, 2018

REFERENCES

Abercrombie, E.D., Keefe, K.A., DiFrischia, D.S., and Zigmond, M.J. (1989). Differential effect of stress on in vivo dopamine release in striatum, nucleus accumbens, and medial frontal cortex. J. Neurochem. *52*, 1655–1658.

Al-Hasani, R., McCall, J.G., Shin, G., Gomez, A.M., Schmitz, G.P., Bernardi, J.M., Pyo, C.-O., Park, S.I., Marcinkiewcz, C.M., Crowley, N.A., et al. (2015). Distinct subpopulations of nucleus accumbens dynorphin neurons drive aversion and reward. Neuron *87*, 1063–1077.

Anstrom, K.K., Miczek, K.A., and Budygin, E.A. (2009). Increased phasic dopamine signaling in the mesolimbic pathway during social defeat in rats. Neuroscience *161*, 3–12.

Badrinarayan, A., Wescott, S.A., Vander Weele, C.M., Saunders, B.T., Couturier, B.E., Maren, S., and Aragona, B.J. (2012). Aversive stimuli differentially modulate real-time dopamine transmission dynamics within the nucleus accumbens core and shell. J. Neurosci. *32*, 15779–15790.

Baliki, M.N., Geha, P.Y., Fields, H.L., and Apkarian, A.V. (2010). Predicting value of pain and analgesia: Nucleus accumbens response to noxious stimuli changes in the presence of chronic pain. Neuron *66*, 149–160.

Ball, G.G. (1970). Hypothalamic self stimulation and feeding: Different time functions. Physiol. Behav. *5*, 1343–1346.

Bassareo, V., De Luca, M.A., and Di Chiara, G. (2002). Differential expression of motivational stimulus properties by dopamine in nucleus accumbens shell versus core and prefrontal cortex. J. Neurosci. *22*, 4709–4719.

Beier, K.T., Steinberg, E.E., DeLoach, K.E., Xie, S., Miyamichi, K., Schwarz, L., Gao, X.J., Kremer, E.J., Malenka, R.C., and Luo, L. (2015). Circuit architecture of VTA dopamine neurons revealed by systematic input-output mapping. Cell *162*, 622–634.

Berridge, K.C., and Kringelbach, M.L. (2008). Affective neuroscience of pleasure: Reward in humans and animals. Psychopharmacology (Berl.) *199*, 457–480.

Berridge, K.C., and Kringelbach, M.L. (2015). Pleasure systems in the brain. Neuron *86*, 646–664.

Berridge, K.C., and Robinson, T.E. (1998). What is the role of dopamine in reward: Hedonic impact, reward learning, or incentive salience? Brain Res. Brain Res. Rev. *28*, 309–369.

Brischoux, F., Chakraborty, S., Brierley, D.I., and Ungless, M.A. (2009). Phasic excitation of dopamine neurons in ventral VTA by noxious stimuli. Proc. Natl. Acad. Sci. USA *106*, 4894–4899.

Bromberg-Martin, E.S., Matsumoto, M., and Hikosaka, O. (2010). Dopamine in motivational control: Rewarding, aversive, and alerting. Neuron *68*, 815–834.

Brooks, A.M., and Berns, G.S. (2013). Aversive stimuli and loss in the mesocorticolimbic dopamine system. Trends Cogn. Sci. *17*, 281–286.

Budygin, E.A., Park, J., Bass, C.E., Grinevich, V.P., Bonin, K.D., and Wightman, R.M. (2012). Aversive stimulus differentially triggers subsecond dopamine release in reward regions. Neuroscience *201*, 331–337.

Daw, N.D., Courville, A.C., and Touretzky, D.S. (2006). Representation and timing in theories of the dopamine system. Neural Comput. *18*, 1637–1677.

Delgado, M.R., Li, J., Schiller, D., and Phelps, E.A. (2008). The role of the striatum in aversive learning and aversive prediction errors. Philos. Trans. R. Soc. Lond. B Biol. Sci. *363*, 3787–3800.

Delgado, M.R., Jou, R.L., and Phelps, E.A. (2011). Neural systems underlying aversive conditioning in humans with primary and secondary reinforcers. Front. Neurosci. *5*, 71.

Deutch, A.Y., and Cameron, D.S. (1992). Pharmacological characterization of dopamine systems in the nucleus accumbens core and shell. Neuroscience *46*, 49–56.

Doya, K. (2008). Modulators of decision making. Nat. Neurosci. *11*, 410–416.

Eshel, N., Tian, J., Bukwich, M., and Uchida, N. (2016). Dopamine neurons share common response function for reward prediction error. Nat. Neurosci. *19*, 479–486.

Fiorillo, C.D. (2013). Two dimensions of value: Dopamine neurons represent reward but not aversiveness. Science *341*, 546–549.

Franklin, K.B.J., and Paxinos, G. (2013). Paxinos and Franklin's The Mouse Brain in Stereotaxic Coordinates (Academic Press).

Gantz, S.C., Ford, C.P., Morikawa, H., and Williams, J.T. (2018). The evolving understanding of dopamine neurons in the substantia nigra and ventral tegmental area. Annu. Rev. Physiol. *80*, 219–241.

Grace, A.A., and Bunney, B.S. (1984). The control of firing pattern in nigral dopamine neurons: Burst firing. J. Neurosci. *4*, 2877–2890.

Hu, H. (2016). Reward and aversion. Annu. Rev. Neurosci. *39*, 297–324.

Jennings, J.H., Sparta, D.R., Stamatakis, A.M., Ung, R.L., Pleil, K.E., Kash, T.L., and Stuber, G.D. (2013). Distinct extended amygdala circuits for divergent motivational states. Nature *496*, 224–228.

Jhou, T.C., Geisler, S., Marinelli, M., Degarmo, B.A., and Zahm, D.S. (2009). The mesopontine rostromedial tegmental nucleus: A structure targeted by the lateral habenula that projects to the ventral tegmental area of Tsai and substantia nigra compacta. J. Comp. Neurol. *513*, 566–596.

Kaufling, J., Veinante, P., Pawlowski, S.A., Freund-Mercier, M.J., and Barrot, M. (2009). Afferents to the GABAergic tail of the ventral tegmental area in the rat. J. Comp. Neurol. *513*, 597–621.

Keiflin, R., and Janak, P.H. (2015). Dopamine prediction errors in reward learning and addiction: From theory to neural circuitry. Neuron *88*, 247–263.

Kempadoo, K.A., Tourino, C., Cho, S.L., Magnani, F., Leinninger, G.-M., Stuber, G.D., Zhang, F., Myers, M.G., Deisseroth, K., de Lecea, L., and Bonci, A. (2013). Hypothalamic neurotensin projections promote reward by enhancing glutamate transmission in the VTA. J. Neurosci. *33*, 7618–7626.

Kim, C.K., Yang, S.J., Pichamoorthy, N., Young, N.P., Kauvar, I., Jennings, J.H., Lerner, T.N., Berndt, A., Lee, S.Y., Ramakrishnan, C., et al. (2016). Simultaneous fast measurement of circuit dynamics at multiple sites across the mammalian brain. Nat. Methods *13*, 325–328.

Lammel, S., Hetzel, A., Häckel, O., Jones, I., Liss, B., and Roeper, J. (2008). Unique properties of mesoprefrontal neurons within a dual mesocorticolimbic dopamine system. Neuron *57*, 760–773.

Lammel, S., Ion, D.I., Roeper, J., and Malenka, R.C. (2011). Projection-specific modulation of dopamine neuron synapses by aversive and rewarding stimuli. Neuron *70*, 855–862.

Lammel, S., Lim, B.K., Ran, C., Huang, K.W., Betley, M.J., Tye, K.M., Deisseroth, K., and Malenka, R.C. (2012). Input-specific control of reward and aversion in the ventral tegmental area. Nature *491*, 212–217.

Lammel, S., Lim, B.K., and Malenka, R.C. (2014). Reward and aversion in a heterogeneous midbrain dopamine system. Neuropharmacology *76*, 351–359.

Lerner, T.N., Shilyansky, C., Davidson, T.J., Evans, K.E., Beier, K.T., Zalocusky, K.A., Crow, A.K., Malenka, R.C., Luo, L., Tomer, R., and Deisseroth, K. (2015). Intact-brain analyses reveal distinct information carried by SNc dopamine subcircuits. Cell *162*, 635–647.

Lerner, T.N., Ye, L., and Deisseroth, K. (2016). Communication in neural circuits: Tools, opportunities, and challenges. Cell *164*, 1136–1150.

Li, Y., Zeng, J., Zhang, J., Yue, C., Zhong, W., Liu, Z., Feng, Q., and Luo, M. (2018). Hypothalamic Circuits for predation and evasion. Neuron *97*, 911–924.

Liu, Z., Zhou, J., Li, Y., Hu, F., Lu, Y., Ma, M., Feng, Q., Zhang, J.-E., Wang, D., Zeng, J., et al. (2014). Dorsal raphe neurons signal reward through 5-HT and glutamate. Neuron *81*, 1360–1374.

Lloyd, K., and Dayan, P. (2016). Safety out of control: Dopamine and defence. Behav. Brain Funct. *12*, 15.

Martinez, R.C.R., Oliveira, A.R., Macedo, C.E., Molina, V.A., and Brandão, M.L. (2008). Involvement of dopaminergic mechanisms in the nucleus accumbens core and shell subregions in the expression of fear conditioning. Neurosci. Lett. *446*, 112–116.

Matsumoto, M., and Hikosaka, O. (2007). Lateral habenula as a source of negative reward signals in dopamine neurons. Nature *447*, 1111–1115.

Matsumoto, M., and Hikosaka, O. (2009). Two types of dopamine neuron distinctly convey positive and negative motivational signals. Nature *459*, 837–841.

McCutcheon, J.E., Ebner, S.R., Loriaux, A.L., and Roitman, M.F. (2012). Encoding of aversion by dopamine and the nucleus accumbens. Front. Neurosci. *6*, 137.

McDevitt, R.A., Tiran-Cappello, A., Shen, H., Balderas, I., Britt, J.P., Marino, R.A.M., Chung, S.L., Richie, C.T., Harvey, B.K., and Bonci, A. (2014).

Serotonergic versus nonserotonergic dorsal raphe projection neurons: Differential participation in reward circuitry. Cell Rep. *8*, 1857–1869.

Menegas, W., Babayan, B.M., Uchida, N., and Watabe-Uchida, M. (2017). Opposite initialization to novel cues in dopamine signaling in ventral and posterior striatum in mice. eLife *6*, e21886.

Mirenowicz, J., and Schultz, W. (1996). Preferential activation of midbrain dopamine neurons by appetitive rather than aversive stimuli. Nature *379*, 449–451.

Morales, M., and Margolis, E.B. (2017). Ventral tegmental area: Cellular heterogeneity, connectivity and behaviour. Nat. Rev. Neurosci. *18*, 73–85.

Nieh, E.H., Vander Weele, C.M., Matthews, G.A., Presbrey, K.N., Wichmann, R., Leppla, C.A., Izadmehr, E.M., and Tye, K.M. (2016). Inhibitory input from the lateral hypothalamus to the ventral tegmental area disinhibits dopamine neurons and promotes behavioral activation. Neuron *90*, 1286–1298.

Osakada, F., and Callaway, E.M. (2013). Design and generation of recombinant rabies virus vectors. Nat. Protoc. *8*, 1583–1601.

Patriarchi, T., Cho, J.R., Merten, K., Howe, M.W., Marley, A., Xiong, W.-H., Folk, R.W., Broussard, G.J., Liang, R., Jang, M.J., et al. (2018). Ultrafast neuronal imaging of dopamine dynamics with designed genetically encoded sensors. Science *360*, eaat4422.

Peciña, S., and Berridge, K.C. (2005). Hedonic hot spot in nucleus accumbens shell: Where do mu-opioids cause increased hedonic impact of sweetness? J. Neurosci. *25*, 11777–11786.

Qi, J., Zhang, S., Wang, H.-L., Wang, H., de Jesus Aceves Buendia, J., Hoffman, A.F., Lupica, C.R., Seal, R.P., and Morales, M. (2014). A glutamatergic reward input from the dorsal raphe to ventral tegmental area dopamine neurons. Nat. Commun. *5*, 5390.

Roeper, J. (2013). Dissecting the diversity of midbrain dopamine neurons. Trends Neurosci. *36*, 336–342.

Roitman, M.F., Stuber, G.D., Phillips, P.E.M., Wightman, R.M., and Carelli, R.M. (2004). Dopamine operates as a subsecond modulator of food seeking. J. Neurosci. *24*, 1265–1271.

Salamone, J.D. (1994). The involvement of nucleus accumbens dopamine in appetitive and aversive motivation. Behav. Brain Res. *61*, 117–133.

Salamone, J.D., and Correa, M. (2012). The mysterious motivational functions of mesolimbic dopamine. Neuron *76*, 470–485.

Salamone, J.D., Correa, M., Mingote, S.M., and Weber, S.M. (2005). Beyond the reward hypothesis: Alternative functions of nucleus accumbens dopamine. Curr. Opin. Pharmacol. *5*, 34–41.

Schultz, W. (2016). Dopamine reward prediction-error signalling: A two-component response. Nat. Rev. Neurosci. *17*, 183–195.

Schwartzbaum, J.S., and Leventhal, T.O. (1990). Neural substrates of behavioral aversion in lateral hypothalamus of rabbits. Brain Res. *507*, 85–91.

Seymour, B., O'Doherty, J.P., Koltzenburg, M., Wiech, K., Frackowiak, R., Friston, K., and Dolan, R. (2005). Opponent appetitive-aversive neural processes underlie predictive learning of pain relief. Nat. Neurosci. *8*, 1234–1240.

Seymour, B., Daw, N., Dayan, P., Singer, T., and Dolan, R. (2007). Differential encoding of losses and gains in the human striatum. J. Neurosci. *27*, 4826–4831.

Sorg, B.A., Davidson, D.L., Hochstatter, T., and Sylvester, P.W. (2002). Repeated cocaine decreases the avoidance response to a novel aversive stimulus in rats. Psychopharmacology (Berl.) *163*, 9–19.

Stamatakis, A.M., Van Swieten, M., Basiri, M.L., Blair, G.A., Kantak, P., and Stuber, G.D. (2016). Lateral hypothalamic area glutamatergic neurons and their projections to the lateral habenula regulate feeding and reward. J. Neurosci. *36*, 302–311.

Starkweather, C.K., Gershman, S.J., and Uchida, N. (2018). The medial prefrontal cortex shapes dopamine reward prediction errors under state uncertainty. Neuron *98*, 616–629.

Stauffer, W.R., Lak, A., Yang, A., Borel, M., Paulsen, O., Boyden, E.S., and Schultz, W. (2016). Dopamine neuron-specific optogenetic stimulation in rhesus macaques. Cell *166*, 1564–1571.

Stuber, G.D., Hnasko, T.S., Britt, J.P., Edwards, R.H., and Bonci, A. (2010). Dopaminergic terminals in the nucleus accumbens but not the dorsal striatum corelease glutamate. J. Neurosci. *30*, 8229–8233.

Tan, K.R., Yvon, C., Turiault, M., Mirzabekov, J.J., Doehner, J., Labouèbe, G., Deisseroth, K., Tye, K.M., and Lüscher, C. (2012). GABA neurons of the VTA drive conditioned place aversion. Neuron *73*, 1173–1183.

Tanimoto, H., Heisenberg, M., and Gerber, B. (2004). Experimental psychology: Event timing turns punishment to reward. Nature *430*, 983.

Tian, J., and Uchida, N. (2015). Habenula lesions reveal that multiple mechanisms underlie dopamine prediction errors. Neuron *87*, 1304–1316.

Tian, J., Huang, R., Cohen, J.Y., Osakada, F., Kobak, D., Machens, C.K., Callaway, E.M., Uchida, N., and Watabe-Uchida, M. (2016). Distributed and mixed information in monosynaptic inputs to dopamine neurons. Neuron *91*, 1374–1389.

Ungless, M.A., Magill, P.J., and Bolam, J.P. (2004). Uniform inhibition of dopamine neurons in the ventral tegmental area by aversive stimuli. Science *303*, 2040–2042.

Wassum, K.M., Ostlund, S.B., and Maidment, N.T. (2012). Phasic mesolimbic dopamine signaling precedes and predicts performance of a self-initiated action sequence task. Biol. Psychiatry *71*, 846–854.

Watabe-Uchida, M., Eshel, N., and Uchida, N. (2017). Neural circuitry of reward prediction error. Annu. Rev. Neurosci. *40*, 373–394.

Weissbourd, B., Ren, J., DeLoach, K.E., Guenthner, C.J., Miyamichi, K., and Luo, L. (2014). Presynaptic partners of dorsal raphe serotonergic and GABAergic neurons. Neuron *83*, 645–662.

Wise, R.A. (2004). Dopamine, learning and motivation. Nat. Rev. Neurosci. *5*, 483–494.

Wise, R.A., and Rompre, P.P. (1989). Brain dopamine and reward. Annu. Rev. Psychol. *40*, 191–225.

Yang, C.F., Chiang, M.C., Gray, D.C., Prabhakaran, M., Alvarado, M., Juntti, S.A., Unger, E.K., Wells, J.A., and Shah, N.M. (2013). Sexually dimorphic neurons in the ventromedial hypothalamus govern mating in both sexes and aggression in males. Cell *153*, 896–909.

Yang, H., de Jong, J.W., Tak, Y., Peck, J., Bateup, H.S., and Lammel, S. (2018). Nucleus accumbens subnuclei regulate motivated behavior via direct inhibition and disinhibition of VTA dopamine subpopulations. Neuron *97*, 434–449.

Young, A.M.J. (2004). Increased extracellular dopamine in nucleus accumbens in response to unconditioned and conditioned aversive stimuli: Studies using 1 min microdialysis in rats. J. Neurosci. Methods *138*, 57–63.

STAR★METHODS

KEY RESOURCES TABLE

REAGENT or RESOURCE	SOURCE	IDENTIFIER
Antibodies		
Anti-TH mouse monoclonal antibody	Millipore	Cat#: MAB318; RRID: AB_2201528
Anti-TH rabbit polyclonal antibody	Millipore	Cat#: 657012; RRID: AB_696697
Streptavidin, Alexa Fluor 488 conjugate	Thermo Fisher Scientific	Cat#: S32354; RRID: AB_2315383
Goat anti-rabbit IgG(H+L), Alexa Fluo 546 secondary antibody	Thermo Fisher Scientific	Cat#: A-11035; RRID: AB_143051
Goat anti-mouse IgG(H+L), Alexa Fluo 546 secondary antibody	Thermo Fisher Scientific	Cat#: A-11003; RRID: AB_2534071
Goat anti-rabbit IgG(H+L), Alexa Fluor 647 secondary antibody	Thermo Fisher Scientific	Cat#: A-21244; RRID: AB_141663
Goat anti-mouse IgG(H+L), Alexa Fluor 647 secondary antibody	Thermo Fisher Scientific	Cat#: A-21235; RRID: AB_141693
Bacterial and Virus Strains		
AAV-hSyn-hChR2(H134R)-eYFP	UNC Vector Core	N/A
AAV-EF1a-DIO-hChR2(H134R)-eYFP	UNC Vector Core	N/A
AAV-EF1a-DIO-hChR2(H134R)-mCherry	UNC Vector Core	N/A
AAV-EF1a-DIO-eNpHR3.0-eYFP	UNC Vector Core	N/A
AAV-EF1a-DIO-eYFP	UNC Vector Core	N/A
AAV-EF1a-DIO-mCherry	UNC Vector Core	N/A
AAV-hSyn-EYFP	UNC Vector Core	N/A
AAV-EF1a-DIO-GCaMP6m	Stanford Gene Vector and Virus Core	GVVC-AAV-95
AAV-EF1a-FLEX-TVA-mCherry	UNC Vector Core	N/A
AAV-CA-FLEX-RG	UNC Vector Core	N/A
Rabies EnvA-ΔG-GFP	Gift from Kevin Beier, UC Irvine	N/A
AAV-flex-taCasp3-TEVp	UNC Vector Core	N/A
AAV-Syn-dLight1.1	Gift from Lin Tian, UC Davis	N/A
Chemicals		
CNQX	Bio-tech	CAS: 479347-85-8
Picrotoxin	Sigma	CAS: 124-87-8
D-AP5	Fisher Scientific	Cat#:01-061-00
Neurobiotin Tracer	Vector lab	Cat#:SP-1120
Red retrobeads IX	Lumafluor	Item#: R170
Green retrobeads IX	Lumafluor	Item#:G180
Experimental Models: Organisms/Strains		
Mouse: B6.SJL-Slc6a3$^{tm1.1(cre)Bkmn}$/J	The Jackson Laboratory	RRID: IMSR_JAX:006660
Mouse: STOCK Tg(Slc17a8-icre)1Edw/SealJ	The Jackson Laboratory	RRID: IMSR_JAX:018147
Mouse: STOCK *Slc17a6*$^{tm2(cre)Lowl}$/J	The Jackson Laboratory	RRID: IMSR_JAX:016963
Mouse: Gad2$^{tm2(cre)Zjh}$/J	The Jackson Laboratory	RRID: IMSR_JAX:010802
Mouse: B6129S6 Gt(ROSA)26Sor$^{tm14(CAG-tdTomato)Hze}$/J	The Jackson Laboratory	RRID: IMSR_JAX: 007908
Mouse: C57BL/6J	The Jackson Laboratory	RRID: IMSR_JAX:000664

CONTACT FOR REAGENT AND RESOURCE SHARING

Further information and requests for resources and reagents should be directed to and will be fulfilled by the Lead Contact, Stephan Lammel (lammel@berkeley.edu).

EXPERIMENTAL MODEL AND SUBJECT DETAILS

The following mouse lines (25-30 g, 8-12 weeks old, male) were used for the experiments: C57Bl6 mice (Jackson Laboratory), DAT::IRES-Cre (Jackson Laboratory, stock number: *006660*, strain code: B6.SJL-Slc6a3tm1.1(cre)Bkmn/J), VGLUT2::IRES-Cre (Jackson Laboratory, stock number: *016963*, strain code: Slc17a6tm2(cre)Lowl/J), VGLUT3::IRES-Cre (Jackson Laboratory, stock number: 018147, strain code: Tg(Slc17a8-icre)1Edw/SealJ), GAD2::IRES-Cre (Jackson Laboratory, stock number: 010802, strain code: $Gad2^{tm2(cre)Zjh}$/J), Ai14 Cre reporter mice (Jackson Laboratory, stock number: 007908, strain code: B6;129S6 Gt(ROSA) $26Sor^{tm14(CAG-tdTomato)Hze}$/J). Ai14 Cre reporter mice were crossed to GAD2::IRES-Cre and VGLUT2::IRES-Cre mice. Mice were maintained on a 12:12 light cycle (lights on at 07:00). All procedures complied with the animal care standards set forth by the National Institutes of Health and were approved by University of California Berkeley's Administrative Panel on Laboratory Animal Care.

METHOD DETAILS

Stereotaxic surgeries

As previously described (Lammel et al., 2008, 2012), all stereotaxic injections were performed under general ketamine–dexmedetomidine anesthesia using a stereotaxic instrument (Kopf Instruments, Model 1900). For red/green fluorescent retrobead labeling, mice were injected unilaterally with fluorescent retrobeads (80-100 nl; LumaFluor Inc.) in the nucleus accumbens (NAc) ventromedial shell (vNAcMed, bregma: 1.5 mm, lateral: 0.9 mm, ventral: −4.8 mm) and/or NAc lateral shell (NAcLat, bregma: 0.98 mm, lateral: 2 mm, ventral: −4.2 mm), ventral tegmental area (VTA, bregma: −3.4 mm, lateral: 0.3 mm, ventral: −4.5 mm), lateral habenula (LHb, bregma: −1.6 mm, lateral: 0.5 mm, ventral: −3.2 mm) or periaqueductal gray (PAG, bregma: −4.2 mm, lateral: 0 mm, ventral: −2.6 mm) using a 1 μl Hamilton syringe (Hamilton). The AAVs (adeno associated virus) used in this study were from the Deisseroth laboratory (AAV5-eNpHR3.0-eYFP; AAV5-EF1α–DIO-hChR2(H134R)-eYFP; AAV5-EF1α-DIO-eYFP; AAVDJ-DIO-GcAMP6m; AAV-DJ-hSyn-GCaMP6m; AAV5-EF1a-DIO-hChR2(H134R)-mCherry; $\sim 10^{12}$ infectious units per ml, prepared by the University of North Carolina Vector Core or the Stanford Gene Vector and Virus Core), from the Uchida lab (Harvard) (AAV5-flex-RG; AAV5-flex-TVA-mCherry; $\sim 10^{12}$ infectious units per ml; prepared by the University of North Carolina Vector Core Facility) or from the Shah lab (UCSF) (AAV5-flex-taCasp3-TEVp; $\sim 10^{12}$ infectious units per ml; prepared by the University of North Carolina Vector Core Facility). AAV9-Syn-dLight1.1 was prepared by the Tian lab (UC Davis) and RV-EnvA-ΔG-GFP was from Kevin Beier (Luo lab). For viral injections, 300-500 nL of concentrated virus solution was injected into the NAcLat, vNAcMed, VTA (same coordinates as above), dorsal raphe nucleus (DR, bregma: −4.4 mm, lateral: 0 mm, ventral: −3.2 mm) or the lateral hypothalamus (LH, bregma: −0.8 mm, lateral: 1 mm, ventral: −5.4 mm) using a syringe pump (Harvard Apparatus) at 150 nl/min. The injection needle was withdrawn 10 min after the end of the infusion. For *in vivo* optogenetic experiments, mice received unilateral (ChR2 experiments) or bilateral (NpHR experiments) implantation of a chronically implanted optical fiber (200 μm, NA = 0.22, Doric Lenses Inc.; NA = 0.37, Newdoon Inc.) dorsal to the VTA (bregma: −3.4 mm, lateral: ± 0.3 mm, ventral: −4.2 mm). For *in vivo* fiber photometry experiments, mice received unilateral implantation of a chronically implanted optical fiber (400 μm, NA = 0.48; Doric Lenses Inc.) in the VTA (bregma: −3.4 mm, lateral: 0.3 mm, ventral: −4.5 mm) or dual optical fibers in the vNAcMed (bregma: 1.5 mm, lateral: ± 0.9 mm, ventral: −4.8 mm) or dorsomedial NAc (dNAcMed, bregma: 1.5 mm, lateral: ± 0.6 mm, ventral: −4.2 mm) or NAcCore (bregma: 1 mm, lateral: ± 1 mm, ventral: −4.2 mm) and NAcLat (bregma: 0.98 mm, lateral: 2 mm, ventral: −4.2 mm) of the same animal. For *in vivo* opto-pharmacology experiments, bilateral infusion guide cannulas (Invivo One) were implanted in the vNAcMed (bregma: 1.5 mm, lateral: ± 0.6 mm, ventral: −3.6 mm). One layer of adhesive cement (C&B Metabond; Parkell) was followed by acrylic (Jet Denture Repair; Lang Dental) to secure the fiber to the skull. The incision was closed with a suture and tissue adhesive (Vetbond; 3M). The animal was kept on a heating pad until it recovered from anesthesia. Experiments were performed 4-8 weeks (for AAVs) or 2-7 days (for retrobeads) after stereotactic injection. Injection sites and optical fiber placements were confirmed in all animals by preparing coronal sections (50-100 μm) of injection and implantation sites. We routinely carried out complete serial reconstruction of the injection sites and optical fiber placements. Although optical fiber placements varied slightly from mouse to mouse, behavioral data from all mice were included in the study.

Electrophysiology

Mice were deeply anaesthetized with pentobarbital (200 mg/kg ip; Vortech). Coronal midbrain slices (200 μm) were prepared after intracardial perfusion with ice-cold artificial cerebrospinal fluid (ACSF) containing (in mM) 50 sucrose, 125 NaCl, 25 $NaHCO_3$, 2.5 KCl, 1.25 NaH_2PO_4, 0.1 $CaCl_2$, 4.9 $MgCl_2$, and 2.5 glucose (oxygenated with 95% O_2/5% CO_2). After 90 min of recovery, slices were transferred to a recording chamber and perfused continuously at 2-4 ml/min with oxygenated ACSF, containing (in mM) 125 NaCl, 25 $NaHCO_3$, 2.5 KCl, 1.25 NaH_2PO_4, 11 glucose, 1.3 $MgCl_2$ and 2.5 $CaCl_2$ at ~30°C. For recording of excitatory postsynaptic currents (EPSCs) picrotoxin (50 μM, Sigma) was added to block inhibitory currents mediated by $GABA_A$ receptors. Cells were visualized with a 40x water-immersion objective on an upright fluorescent microscope (BX51WI; Olympus) equipped with infrared-differential interference contrast video microscopy and epifluorescence (Olympus). Patch pipettes (3.8-4.4 MΩ) were pulled from borosilicate glass (G150TF-4; Warner Instruments) and filled with internal solution, which consisted of (in mM) 117 $CsCH_3SO_3$, 20 HEPES, 0.4 EGTA, 2.8 NaCl, 5 TEA, 4 MgATP, 0.3 NaGTP, 5 QX314, 0.1 Spermine, and 0.1% neurobiotin, pH 7.35 (270–285 mOsm). For recordings of spontaneous firing in VTA dopamine (DA) neurons, the internal solution contained (in mM): 135 K-gluconate, 5 KCl,

10 HEPES, 0.1 EGTA, 2 $MgCl_2$, 2 MgATP, 0.2 NaGTP, and 0.1% neurobiotin, pH 7.35 (290-300 mOsm). Electrophysiological recordings were made using a MultiClamp700B amplifier and acquired using a Digidata 1550 digitizer, sampled at 10 kHz, and filtered at 2 kHz. All data acquisition was performed using pCLAMP software (Molecular Devices). Channelrhodopsin-2 (ChR2) was stimulated by flashing 473 nm light through the light path of the microscope using an ultrahigh-powered light-emitting diode (LED) powered by an LED driver (Prizmatix) under computer control. A dual lamp house adaptor (Olympus) was used to switch between fluorescence lamp and LED light source. The light intensity of the LED was not changed during the experiments and the whole slice was illuminated (5 mW/mm^2). Light-evoked excitatory postsynaptic currents (EPSCs) were obtained every 10 s with one pulse of 473 nm light (5 ms) with neurons voltage clamped at −70 mV. Series resistance (15–25 MΩ) and input resistance were monitored online. For recordings of spontaneous action potential firing, cells were held in current clamp mode and no current injections were made. Spontaneous firing was recorded for at least 3 s before and 5 s after light stimulation (4 Hz or 20 Hz, 5 ms light pulses, 5 mW/mm^2) and averaged over 10 sweeps. For pharmacological experiments, we recorded baseline responses for at least 3-5 min and bath applied 10 μM CNQX (Tocris) for 5-10 min to block AMPA/kainate receptor mediated currents. Data were analyzed offline using MATLAB Software (Mathworks). Light-evoked EPSC amplitudes were calculated by averaging responses from 10 sweeps and then measuring the peak amplitude in a 50 ms window after the light pulse. Cells that did not show a peak in this window that exceeded the baseline noise were classified as non-responders.

DA, glutamate and GABA cells were recorded in both the caudal and rostral VTA. The caudal VTA contained at least some parts of the rostromedial tegmental nucleus (RMTg) (Jhou et al., 2009). The boundary between the VTA and RMTg is difficult to determine, particularly in the caudal VTA, which makes it difficult to determine with certainty whether local inhibitory input to VTA DA neurons originates from within the VTA or from the RMTg. Thus, when referred to in the text, the VTA includes the RMTg, which was originally termed the '*tail of the VTA*' (Kaufling et al., 2009).

In experiments in which we injected red fluorescent retrobeads into both the NAcLat and vNAcMed of the same animal (Figures 3E–3L and 6D–6N), retrogradely labeled neurons projecting to vNAcMed and NAcLat were differentiated according to their anatomical location in the VTA as well as the presence or absence of an I_h current. vNAcMed-projecting DA neurons were mainly located in the medial VTA, while NAcLat-projecting DA neurons are predominantly located in the lateral VTA. In addition, NAcLat-projecting DA neurons possess a prominent I_h current, which is very small or absent in vNAcMed-projecting DA neurons (Lammel et al., 2008, 2011). Although we aimed to selectively target retrobeads to the vNAcMed, several animals also contained labeling in the dNAcMed. Additional retrograde tracing experiment revealed that there were no obvious differences in the anatomical distribution of dNAcMed- and vNAcMed-projecting DA neurons. Both subtypes were located in the medial VTA (data not shown).

To determine the neurochemical identity of the recorded neurons (e.g., TH-immunopositive or -negative cells, tdT-positive/negative GAD2 or VGLUT2 cells), neurons were filled with neurobiotin (Vector) during patch clamp recordings then fixed in 4% paraformaldehyde (PFA) and 24 hours later immunostained for TH. The neurochemical identity was assessed in all experiments and ~80% of all whole-cell patch clamped neurons could be successfully recovered. The DAergic phenotype was confirmed in all recovered cells in which retrogradely labeled VTA neurons projecting to vNAcMed and NAcLat were recorded (a more detailed description on the neurochemical identity of retrogradely labeled neurons in the VTA can be found in (Lammel et al., 2011)).

OPTOGENETICS AND BEHAVIORAL ASSAYS

Aversive Conditioning

Mice with dual fiberoptic implants in the vNAcMed (or dNAcMed or NAcCore) and NAcLat (Figure 1) or single fiberoptic implants in the VTA (Figures 5J–5O) were familiarized with the test chamber (17.8 cm x 12.7 cm x 21.6 cm, Med Associates) for 15 min on the day before the experiment. Two sessions were performed across two days. During the first (conditioning) session, mice were exposed to 10 trials. Each trial consisted of a random interval (30-60 s) followed by a 2 s tone (2.9 kHz, 75 dB), which was immediately followed by a mild (0.4 mA) 2 s electric foot shock delivered through the stainless-steel grid floor. Twenty-four hours later, a second session was performed which consisted of 30 trials in order to further examine the effects of shock omission (10 out of 30 tones (randomly assigned) were not followed by an electric foot shock (67%-foot shock probability).

For aversive conditioning experiments in the head-fixed setup (Figures 8 and S8), mice were first habituated to the setup. Shocks (0.4 mA, 5 ms pulse, 20 Hz for 2 s) were delivered to the tail of the mouse using pre-gelled electrodes (Sonic Technology's adhesive pads for TENS) and a stimulator (SYS-A320, WPI). Tone and shock were controlled by an Arduino microprocessor (Arduino Mega 2560).

Reward Conditioning

To record calcium activity from DA terminals in separate NAc subdivisions during reward conditioning from head-fixed animals (Figure 2), mice were implanted with a custom-made aluminum head plate, held in place with dental cement and acrylic. The head-fixed setup consisted of two horizontal bars that were attached to the head plate and a running disc for the mice to walk or rest on (there was no requirement that the animal move). Water or sucrose solution was delivered via a modified hypodermic needle, and licks were recorded via a custom-made capacitive touch sensor under the control of a microprocessor (Sparkfun Redboard) connected to a digital acquisition box (National Instruments BNC-2090A), which was connected to a computer running MATLAB (Mathworks). Licks were recorded when the tongue of the mouse contacted the metal tubing, which caused an increase in capacitance. Liquid delivery

was controlled using a solenoid (NR research, 161K011). A blue LED and a piezo buzzer producing an 11 kHz tone (Adafruit PS1250) served as cues. The tone was notably different than the one used during the aversive conditioning procedure and did not affect activity in the NAc before conditioning. The solenoid, LED and speaker were controlled by an Arduino microprocessor (Arduino Mega 2560). Mice were habituated to the head-fixed setup during which they received water drops that were not associated with a tone or light cue. After habituation, mice underwent 5 conditioning sessions, which were preceded by a period of water deprivation that lasted for about 16 hours. Mice were tested every other day. Water deprivation did not affect the animal's body weight. Individual sessions lasted for about 1.5 hours and consisted of approximately 100 trials. An individual trial consisted of a 1 s cue (light and tone) followed by a 1 s delay period which ended with delivery of 4 μl of a 1% sucrose solution. Trials were separated by a random delay period that lasted between 30 to 90 s. A trial was considered successful if the mouse consumed the sucrose solution within 3 s of its delivery. For each animal, the first 20 successful trials were pooled and averaged. During the fifth session, 20% of all trials (randomly selected) did not result in sucrose delivery ('reward omission'). In total, each animal was subjected to approximately 500 trials, and calcium signals were simultaneously recorded in the NAcLat and vNAcMed using fiber photometry during all trials.

Real-time Place Preference

Mice with fiberoptic implants were connected to a fiberoptic cable and placed in a custom-made three-compartment chamber (Lammel et al., 2012). The cable was connected to a 473-nm DPSS laser diode (Laserglow) through a rotary adaptor, and laser output was controlled using a Master-8 pulse stimulator (A.M.P.I.). Power output for the cable was tested using a digital power meter (Thorlabs) and was checked before and after each experimental animal; output during light stimulation was estimated to be 5-8 mW/mm^2 at the targeted tissue 200 μm from the fiber tip (https://web.stanford.edu/group/dlab/cgi-bin/graph/chart.php). One randomly assigned side of the chamber was assigned as the initial stimulation side (Phase 1), and after 10 min the stimulation side was switched to the previously non-stimulated side of the chamber (Phase 2). At the start of each session, the mouse was placed in the neutral (middle) compartment, and every time the mouse crossed to the stimulation side, 4 Hz (5 ms pulses) laser stimulation was delivered until the mouse crossed back into the neutral, non-stimulation side. There was no interruption between Phase 1 and Phase 2. The movement of the mice was recorded via a video tracking system (Biobserve) and the time spent in each area (stimulated, non-stimulated, neutral) was calculated.

For the behavioral experiments in Figure S5, a separate cohort of animals was used. Mice received optogenetic stimulation at different frequencies. On the first day, mice received 1 Hz stimulation. The animals performed the same real-time place preference assay that is described above but with omission of Phase 2. 24 hours later, the experiment was performed again, but the stimulation frequency was changed to 2 Hz. On subsequent days, the stimulation frequency was increased to 4 Hz, 10 Hz and 20 Hz. On the last day (day 6), we again tested the mice with 1 Hz stimulation in order to examine if the increase in place preference is specific to the stimulation frequency or caused by conditioning.

Open Field Test

The open-field test was conducted to measure the effect of optogenetic stimulation on general locomotor ability and on anxiety-like behavior. The mice were placed in a custom-made open field chamber (50 × 50 cm) and their movement was recorded and analyzed for 15 min using video-tracking software (Biobserve). Both ChR2 and control (eYFP) mice received 4 Hz (473 nm, 5 ms pulses) optogenetic stimulation during that time. The inner zone of the open-field chamber was defined as the 23 × 23 cm central square area. Mice typically spend very little time in the inner zone; however, in mice that display a robust anxiolytic phenotype, this time would be increased.

Approach-Avoidance Task

To measure avoidance of an unfamiliar aversive stimulus (Sorg et al., 2002), mice were exposed to a rectangular chamber (50 cm x 50 cm for fiber photometry experiments (Figures 5A–5I); 70 cm x 24 cm for eNpHR3.0 experiments (Figures 4G–4M). Mice were first habituated to the chamber for 5 min, after which a piece of cotton dipped in 6% formaldehyde or a novel object was introduced into a randomly assigned side or corner. Typically, mice tend to explore a novel stimulus/object and briefly interact ('sniff') with it. However, in case of formaldehyde, although the animals display strong avoidance behavior, they typically perform multiple approach-avoidance attempts (Videos S3 and S4). For fiber photometry experiments, the first five stimulus interactions were analyzed and averaged to obtain a time-locked response. For optogenetic silencing experiments, 3 min of formaldehyde interaction were recorded using a video tracking software (Biobserve). Both control (eYFP) and NpHR mice were continuously stimulated using a 589 nm DPSS laser (5-8 mW/mm^2 at fiber tip) during the entire session. Location coordinates were imported into MATLAB for analysis. 'Safe' and 'formaldehyde' zones were on opposing sides of the chamber (each 15 × 24 cm). Heatmaps were generated by interpolating the time spent for all locations in the chamber. The maps were then normalized and averaged across all mice. Experimental groups were randomized and investigators were blinded to group allocation (NpHR versus control) as well as outcome assessment. Optogenetic silencing experiments were replicated in a separate cohort of animals. Data from both cohorts were pooled and no animals were excluded (Figure S4B shows injection sites from second cohort of animals).

Opto-pharmacology

For the *in vivo* opto-pharmacology experiments (Figures 7G–7J), VGLUT2-Cre mice received unilateral injection of AAV-DIO-ChR2-eYFP into the LH and were implanted with an optical fiber above the VTA and bilateral infusion cannulas (Invivo One) in the vNAcMed (see Stereotaxic Surgery). Mice received unilateral infusions of either 300 nL saline or 30 ng SCH23390 (D1 receptor antagonist) and 300 ng raclopride (D2 receptor antagonist) dissolved in 300 nL saline 5 min before the real-time place preference experiment. Infusions were at a rate of 150 nl/min and the internal cannula was left in place for 1 min after the infusion. Note that higher doses caused a strong depression of locomotor activity (data not shown). Although we used a very low dose of SCH23390 and raclopride, we still observed some effects on locomotor activity, even though it was not statistically significant. Thus, as an additional control experiment, mice were infused with both antagonists on the contralateral side as we predicted that this would have the same general effect on locomotion but would not attenuate the light-induced aversion as ChR2 expression and light stimulation were unilateral.

FIBER PHOTOMETRY

Calcium transients were measured using a custom-built fiber photometry system as described previously (Kim et al., 2016). Briefly, calcium-dependent fluorescence signals were obtained by stimulating cells expressing GCaMP6m with a 470 nm LED (20 μW at fiber tip) while calcium-independent signals were obtained by stimulating these cells with a 405 nm LED (20 μW at fiber tip). 470 nm and 405 nm LED light were alternated at 20 or 40 Hz and light emission was recorded using an sCMOS Camera (Hamamatsu Flash or Photometrics Prime), which acquired video frames containing the entire fiber bundle (2 fibers, 3 m in length, NA = 0.48, 400 μm core, Doric Lenses) at the same frequency. Video frames were analyzed online and fluorescent signals were acquired using custom acquisition code written in MATLAB based on original code by (Kim et al., 2016). Experimental time stamps were acquired using TTL pulses generated by the video tracking software (Biobserve) or the mouse conditioning chamber (Med Associates). The fluorescent signal obtained after stimulation with 405 nm light was used to correct for movement artifacts as follows: first, the 405 nm signal was fitted to the 470 nm signal using the first and second coefficients of the polynomial that was the best fit (least-squares) to the 470 nm signal. The fitted 405 nm signal was then subtracted from the 470 nm signal to obtain the movement and bleaching-corrected signal (Figures S1B and S1C). Signals were normalized (Z-score) and peri-event plots for the tone-shock trials were generated. Baseline normalization was performed on the original ΔF/F signal using the time-window −2 to 0 s. Thus, Z-scores accurately reflect the number of standard deviations from the mean and it is possible that the baseline is not at zero. AUC for the tone was defined as the integral between 0 and 2 s, whereas AUC for the shock was defined as the integral between 2 and 4 s (Figure 1). For the reward conditioning experiments (Figure 2), AUC for cue onset was calculated over the interval 0-0.5 s, anticipation over the interval 1-2 s and reward delivery over the interval 2-4 s.

For *in vivo opto-photometry* experiments (Figures 7A–7F), VGLUT2-CRE mice were injected with 500 nL AAV-DJ-hSyn-GCaMP6m into the VTA and 500 nL AAV5-EF1a-DIO-hChR2-mCherry into the LH. Optical fibers were implanted in the VTA and vNAcMed or NAcLat. To prevent overlap between ChR2 and GCaMP signals, we 1) used ChR2 that was fused to mCherry and 2) used light at very low intensities: GCaMP excitation was performed using LED light intensities < 20 μW in the vNAcMed or NAcLat and < 2 mW for ChR2 excitation in the VTA. At intervals of 100 s, the mice received laser light stimulation for 10 s at 20 Hz (5 ms pulse-width) in the VTA while we recorded calcium fluorescence signals from vNAcMed or NAcLat terminals using fiber photometry. 20 trials were averaged per animal. The AUC interval was defined as the entire laser stimulation period (0-10 s).

RABIES VIRUS TRACING

We used rabies tracing to map and characterize inputs to different mesolimbic cell populations (Osakada and Callaway, 2013). A limitation of previous rabies tracing studies is that input neurons were often manually counted and not every brain section was analyzed, which can be subjective and limit statistical power, respectively. We therefore combined a rabies virus-based genetic mapping strategy with a semi-automated whole-brain mapping algorithm. Specifically, DAT-Cre were injected with AAV-FLEX-TVA (i.e., a cellular receptor for subgroup A avian leukosis viruses) and AAV-FLEX-RG (i.e., rabies virus glycoprotein) into the VTA and 4 weeks later, 300 nL RV-EnvA-ΔG-GFP (i.e., glycoprotein deficient, GFP expressing rabies virus) was injected into the vNAcMed (n = 4 mice) or NAcLat (n = 5 mice). Although we aimed to target the vNAcMed, we cannot exclude that rabies virus also spread into the dNAcMed. 7 days after injection, mice were perfused with 4% PFA in PBS. Brains were either stored in 30% sucrose in PBS at −80°C or directly processed for analysis. To test the specificity of our rabies virus tracing approach, we injected RV-EvnA-ΔG-GFP into the vNAcMed of three mice that were not previously injected with FLEX-TVA or FLEX-RG. In this case we did not observe any GFP-positive cells in either the vNAcMed or in the VTA (data not shown).

For input mapping, 75 μm sections of the whole brain were prepared and scanned using a Zeiss Axio Scan Z1. Individual slices were aligned using customized MATLAB scripts. GFP-positive pixels were identified on the basis of a pixel-intensity threshold in the green channel (Figure S3A). False-positive pixels (artifacts) were manually removed. Positive pixels were assigned to different brain areas based on "*The Mouse Brain in Stereotaxic Coordinates*" (Franklin and Paxinos, 2013) (Figure S3B). Pixels per zone were then represented as a percentage of all inputs. 12 brain regions were randomly selected to validate this method and a human

observer counted GFP-positive cells in these regions. These results demonstrated a high correlation between manually scoring of input neurons by an independent observer and our automated segmentation procedure (Figure S3C; R2 = 0.956, $p < 0.001$, n = 12 brain regions).

IN SITU HYBRIDIZATION

To determine the genetic identity of presynaptic LH neurons synapsing onto distinct VTA cell populations, we combined transsynaptic rabies tracing (above) with *in situ* hybridization. Probe sequence for the VGLUT2 DIG RNA probe as well as the free floating *in situ* protocol were adapted from (Weissbourd et al., 2014). Briefly, 100 μm sections were washed in diethyl pyrocarbonate (DEPC)-treated PBS and treated with a 7 μg/ml proteinase K solution for 10 min at 37°C. Proteinase K was inactivated using 4% PFA in PBS, which was followed by washing in PBS and acetylation in 0.25% acetic anhydride in 0.1 M triethanolamine in DEPC-treated water. Tissue sections were incubated overnight in hybridization solution (50% deionized formamide, 1x Denhardt's, 10% Dextran sulfate and 5x Saline-Sodium Citrate (SSC)) with 100 ng/ml probe at 55°C. Stringency washes were in 2x SSC with 50% formamide for 1 hour, and in 2x SSC and 0.2x SSC for 20 min, each at 65°C. This was followed by blocking for 1 hour in DIG blocking buffer (Roche) and overnight incubation at 25°C in 1:1000 Anti-Digoxigenin-AP FAB fragments (Roche). Because the *in situ* hybridization procedure attenuates fluorescence, tissue sections were co-stained with a chicken anti-GFP (1:1000, Abcam). Primary antibody incubation was for 2 hours and was followed by washing steps in DIG wash buffer (Roche) and incubation with secondary antibodies (Alexa Fluor 546 goat anti-rabbit, Alexa Fluor 647 goat anti-mouse (all 1:750, Thermo Fisher Scientific) and Alexa Fluor 477 goat anti-chicken (1:750, Abcam) as well as the alkaline phosphatase substrate reacting with NBT/BCIP in detection buffer (Roche). Slides were imaged on a Zeiss AxioImager M2 microscope using a 20x objective. GFP- and VGLUT2-positive cells in the LH were manually counted using ImageJ.

HISTOLOGY AND MICROSCOPY

Immunofluorescence and confocal microscopy were performed as described previously (Lammel et al., 2008, 2012). Briefly, after intracardial perfusion with 4% paraformaldehyde in PBS, pH 7.4, the brains were post-fixed overnight and coronal midbrain sections (50 or 100 μm) were prepared. Sections were stained overnight in primary antibodies (rabbit anti-tyrosine hydroxylase (TH, 1:1000, Millipore), mouse anti-TH (1:1000, Millipore) and rabbit anti-c-*fos* (1:500, Santa Cruz Biotechnology)). The next day, sections were stained for 2 hours in secondary antibodies (Alexa Fluor 546 goat anti-rabbit, Alexa Fluor 546 goat anti-mouse, Alexa Fluor 647 goat anti-rabbit, Alexa Fluor 647 goat anti-mouse (1:750, Thermo Fisher Scientific) and Alexa Fluor 477 goat anti-chicken (1:750, Abcam)). Image acquisition was performed with Zeiss LSM710 laser scanning confocal microscope using 20x or 40x objectives and on a Zeiss AxioImager M2 upright widefield fluorescence/differential interference contrast microscope with charge-coupled device camera using 5x objectives. Confocal images were analyzed using ImageJ. Sections were labeled relative to bregma using landmarks and neuroanatomical nomenclature as described in "*The Mouse Brain in Stereotaxic Coordinates*" (Franklin and Paxinos, 2013).

For quantification of fluorescence intensities (Figures 3F, 3G, 6E, and 6F) confocal images were acquired using a 60x objective with identical pinhole, dwell time, gain and laser settings. Twenty-two images from 11 mice (LH → VTA, n = 6 mice; DR → VTA, n = 5 mice) from the medial and lateral VTA (same section) were acquired at the same focal level. The medial and lateral VTA was defined as the area that corresponds to the anatomical location of distinct DA subpopulations (Lammel et al., 2008, 2011). The medial VTA was defined as the region comprising the paranigral nucleus and interfascicular nucleus, whereas the lateral VTA was defined as the lateral parabrachial pigmented nucleus and the medial lemniscus region adjacent to the substantia nigra. No additional post-processing was performed on any of the collected images. Fluorescence pixel intensity was then quantified in each VTA subregion using ImageJ software.

For quantification of *fos* immunoreactivity (Figure S7), VGLUT2-Cre::tdTomato mice were placed in an open field chamber (50 × 50 cm) and exposed to a cotton swab that was dipped in 6% formaldehyde (form) or water (ctrl). Mice were perfused with 4% PFA 45 min later, and immunohistochemistry was performed 24 hours later. Animals were randomized and investigators were blind to group allocation (form versus ctrl) and outcome assessments.

QUANTIFICATION AND STATISTICAL ANALYSIS

Student's t tests (paired and unpaired), Mann-Whitney U test (for samples that are not normally distributed), and one- and two-way ANOVAs were used to determine statistical differences for anatomical, behavioral and electrophysiological data using GraphPad Prism 6 (Graphpad Software). Holm-Sidak or Tukey HSD post hoc analysis was applied, when applicable, to correct for multiple comparisons. Statistical significance was * $p < 0.05$, ** $p < 0.01$, *** $p < 0.001$. All data are presented as means ± SEM. For each experiment we describe the statistics in the main text. "n" always refers to the number of mice with the exception of the *ex vivo* electrophysiology experiments (Figures 3H–3L and 6G–6N). In this case "n" refers to the number of cells and the number of mice used is reported in the main text.

Results described throughout the paper were reproduced. First, optogenetic stimulation experiments using the RT place preference assay were replicated in separate cohorts of wild-type mice (using an AAV that expresses ChR2 under control of the CaMKII

promoter) for stimulation of LH (Figures 4A–4F) and DR (Figures 3M–3P) inputs to the VTA. Second, optogenetic silencing experiments (Figures 4G–4M) were replicated in three separate cohorts of animals. The first cohort was a pilot experiment using a small group of animals in an open field area. The other two cohorts were larger groups using a rectangular chamber and data from the latter two cohorts were pooled. Third, *ex vivo* slice recordings for determining synaptic connectivity of LH (Figures 6G–6K) and DR (Figures 3H–3L) inputs with VTA DA subpopulations were replicated in wild-type mice (using an AAV that expresses ChR2 under control of the CaMKII promoter). Fourth, fiber photometry experiments using the aversive conditioning assay (Figure 1) were replicated in DAT-Cre mice in which either vNAcMed or NAcLat was targeted. Figure 1 includes only mice in which simultaneous recordings from both vNAcMed and NAcLat were performed, but we present an overview in Figure 1L. No issues were identified in replicating any of the reported findings.

Investigators were blinded to allocation of groups and outcome assessment for experiments in Figures 3A–3D, 3M–3P, 4, S3A–S3C, S5H–S5K, S6, and S7. All other experiments were not blinded. All custom code used for analysis in this manuscript is available on request.

Neuron, Volume *101*

Supplemental Information

A Neural Circuit Mechanism for Encoding Aversive Stimuli in the Mesolimbic Dopamine System

Johannes W. de Jong, Seyedeh Atiyeh Afjei, Iskra Pollak Dorocic, James R. Peck, Christine Liu, Christina K. Kim, Lin Tian, Karl Deisseroth, and Stephan Lammel

Supplemental Material: de Jong, Afjei et al.

Figure S1. *In vivo* dual fiber photometry of DA terminals across different NAc subregions during aversive conditioning, Related to Figure 1.
(A) Freezing in response to the tone before conditioning (first shock trial) and after conditioning (last shock trial; first: 14.40 ± 9.27%, n=5; last: 80.60 ± 10.78%, n = 5; ** $p < 0.01$, paired Student's t-test; data represent means ± SEM).
(B, C) Representative examples of raw 470 nm and fitted 405 nm signals from DA terminals simultaneously recorded in the NAcLat (B) and vNAcMed (C). Note that the fitted 405 nm signal is subtracted from the 470 nm signal to obtain the movement- and bleaching-corrected signal (as shown in **Figure 1 and Supplementary Movie 1**).
(D) Although the area under the curve during shock exposure was not significantly different in ventral NAcMed DA terminals (**Figure 1I**, inset), we observed a significant phasic increase in fluorescence activity immediately after shock onset compared to omission trials (Shock: 1.38 ± 0.20; Omission: 0.98 ± 0.13, n = 11 mice; * $p < 0.05$, paired Student's t-test). This is consistent with an aversion prediction error as shock occurrence was uncertain (67%-foot shock probability; data represent means ± SEM).
(E) Coronal brain section showing DA terminals expressing GCaMP6m (green), TH-immunostaining (red) and location of fiber implants in the NAcLat, ventral NAcMed, dorsal NAcMed and NAcCore as well as a sample fluorescence image showing fiber placement from a recording that lacked an excitatory or inhibitory response to foot shock (ac: anterior commissure; scale bars: 200 μm). N = 2 mice lacked an excitatory or inhibitory response to foot shock. These animals had recording-sites that were outside the ventral striatal target region.

Figure S2. Average Z-score responses for individual, well-trained animals during a reward conditioning trial, Related to Figure 2.
Simultaneous recordings from individual animals in the NAcLat (A) and ventral NAcMed (B) that were used for the data shown in Figure 2.

Figure S3. Monosynaptic rabies virus tracing of vNAcMed- and NAcLat-projecting DA neurons using automated segmentation arithmetic, Related to Figure 3.
(A) Fluorescence images showing GFP-positive cells in the ventral striatum (left) and automated segmentation (right, positive pixels in white; scale bar: 50 μm).
(B) Segmented pixels were semi-automatically assigned to defined brain structures, e.g., LH (top), VTA (middle) and DR (bottom). Designated pixels are in red while other GFP-positive pixels are in white (scale bar: 500 μm).
(C) Graph showing high correlation between manually scoring of input neurons by an independent observer and the automated segmentation procedure.
(D) vNAcMed-projecting starter cells were located in the ventromedial VTA (mVTA, green, left panel, IPN: interpeduncular nucleus). Starter cell populations in the VTA were defined as GFP- and TVA-mCherry-positive cells. Bar graph shows co-localization analysis of starter cells with TH (100% TH-immunopositive), non-starter TVA-mCherry-positive cells (100% TH-immunopositive) and secondary (TVA-mCherry-negative) cells (6.52% TH-immunopositive). The right panel shows a sample confocal image of vNAcMed-projecting starter cells (green: RV-ΔG-GFP, red: TVA-mCherry, blue: TH; scale bar: 10 μm).
(E) Same as in (D) but for NAcLat-projecting starter cells, which were mainly located in the

lateral VTA (lVTA). Starter cells and TVA-mCherry-positive cells were 100% TH-immunopositive, while secondary cells were 13.5% TH-immunopositive.

Abbreviations used in Figure 3D: OFC: orbital frontal cortex, mPFC: medial prefrontal cortex, DMS: dorsomedial striatum, DLS: dorsolateral striatum, VP: ventral pallidum, BNST: bed nucleus of the stria terminalis, GP: globus pallidus, PO: preoptic area, LH: lateral hypothalamus, PVN: periventricular nucleus, CeA: central amygdala, LHb: lateral habenula, MHb: medial habenula, STh: subthalamic nucleus, DR: dorsal raphe nucleus, LDT: laterodorsal tegmentum, LPB: lateral parabrachial nucleus.

Figure S4. Serial reconstructions of viral injection sites and anatomical locations of optical fiber implants, Related to Figures 4 and 5.
(A) Coronal brain sections showing ChR2-eYFP (green) expression in the lateral hypothalamus (LH). Top: Left panels show representative examples of ChR2-eYFP injection sites across the rostro-caudal extent of the LH. Right panels show schematics of the corresponding brain regions in which ChR2-eYFP was detected. Each color represents the expression profile from a single mouse that was used for the experiments shown in **Figures 4A-4F**. Blue color code represents example images shown in the left panels (scale bar: 500 μm, f: fornix, LPO: lateral preoptic area). Bottom: Schematics showing anatomical location of fiber implants in the midbrain.
(B, C) Same as in (A) but for NpHR3.0-eYFP expression in the LH of individual mice used for the experiments shown in **Figures 4G-4M** (B) and for GCaMP6m expression in the LH of individual mice used for the experiments shown in **Figures 5A-5I** (C). Note that fiber implants for optogenetic experiments (A, B) were placed 0.3-0.5 mm above the VTA, while fiber photometry experiments (C) required fiber implants to be placed within the VTA.

Figure S5. Optogenetic stimulation of LH_{VGLUT2} inputs to VTA does not affect locomotor activity or anxiety but promotes aversion in a frequency dependent manner, Related to Figure 4.
(A) Schematic of real-time place preference assay, which was performed over 6 days. Each day ChR2-expressing LH_{VGLUT2} inputs to VTA were stimulated using a different frequency.
(B-G) There was no effect on place preference behavior for 1 Hz optogenetic stimulation (B; stim: 286.4 ± 48.92 s; non-stim.: 214.4 ± 36.43 s, n = 8 mice; $p = 0.416$, paired Student's t-test), whereas increasing stimulation frequencies to 2 Hz (C; stim: 134.6 ± 17.19 s; non-stim.: 382.5 ± 31.51 s, n = 8 mice; ** $p < 0.01$, paired Student's t-test), 4 Hz (D; stim: 100.1 ± 21.22 s; non-stim.: 398.8 ± 35.76 s, n = 8 mice; *** $p < 0.001$, paired Student's t-test), 10 Hz (E; stim: 68.74 ± 12.24 s; non-stim.: 465.1 ± 22.53 s, n = 8 mice; *** $p < 0.001$, paired Student's t-test) and 20 Hz (F; stim: 26.13 ± 4.69 s; non-stim.: 512.4 ± 13.45 s, n = 8 mice; *** $p < 0.001$, paired Student's t-test) caused an increase place avoidance behavior. Note that the increase in place avoidance behavior was not due to conditioning, as repeating 1 Hz stimulation (G; stim: 240.6 ± 36.44 s; non-stim.: 282.7 ± 35.16 s, n = 8 mice; $p = 0.571$, paired Student's t-test) on day 6 did not promote place aversion (data represent means ± SEM).
(H) Schematic of open field test for assessing general locomotor activity and anxiety behavior, which involves 4 Hz light stimulation of ChR2- or eYFP expressing LH_{VGLUT2} terminals in the VTA for 15 min.
(I) Representative trajectories of animals expressing ChR2 (top) or eYFP (bottom) in LH_{VGLUT2} terminals. (J) Bar graph showing no significant difference in total distance traveled (a measure of

locomotor activity) between ChR2 and eYFP groups (ChR2: 3232 ± 500.5 cm, n = 9 mice; eYFP: 3078 ± 490.5 cm, n = 10 mice; p = 0.83, unpaired Student's t-test; data represent means ± SEM).
(K) Bar graph showing no significant difference in time spent in center area (a measure of anxiety-related behavior) between ChR2 and eYFP groups (Center: ChR2: 88.76 ± 20.79 s, n = 9 mice; eYFP: 77.41 ± 19.60 cm, n = 10 mice; Corners: ChR2: 506.43 ± 50.45 s n = 9 mice; eYFP: 577.69 ± 51.84 cm, n = 10 mice; $p_{interaction}$ = 0.418, F(1,17) = 0.689, two-way RM ANOVA; Data represent means ± SEM).

Figure S6. LH neurons projecting to VTA and LHb represent largely independent projections, Related to Figure 4.
(A) Schematic showing dual injection of fluorescent retrobeads with distinct fluorophores into VTA and lateral habenula (LHb) of the same animal.
(B) Confocal images showing retrogradely labeled LH neurons projecting to LHb (green beads) and LH neurons projecting to VTA (red beads) using a 10x (upper row; scale bar: 100 μm) and 40x objective (lower row; scale bar: 20 μm).
(C) Bar graph showing that most LH neurons contain either red beads (i.e., cells that project to VTA, red bar, 62%, n = 84/135 cells) or green beads (i.e., cells that project to LHb, green bar, n = 48/135 cells). Only 2% of LH neurons are double labeled (i.e., cells that contain both red and green beads, yellow bar, n = 3/135 cells; n = 3 mice). Inset shows an example of a double-labeled LH neuron (scale bar: 20 μm).
(D-F) Same experimental design as in (A-C) but for retrobead injections into the VTA and periaqueductal gray (PAG). The bar graph shows that most LH neurons contain either red beads (i.e., cells that project to VTA, red bar, 51%, n = 152/296 cells) or green beads (i.e., cells that project to PAG, green bar, 48%, n = 141/296 cells). Only 1% of LH neurons are double labeled (i.e., cells that contain both red and green beads, yellow bar, n = 3/296 cells; n = 3 mice).

Figure S7. Selective fos immunoreactivity in LH_{VGLUT2} neurons projecting to VTA in response to an aversive stimulus, Related to Figure 5.
(A) Schematic showing injection of green retrobeads into the VTA of VGLUT2-Cre::tdTomato mice (upper panel), experimental timeline (middle panel) and coronal section showing retrobead (green) injection site in the VTA (lower panel; scale bar: 100 μm).
(B, C) Confocal image showing retrogradely labeled (green, beads) glutamatergic (tdT-positive, red) LH neurons that project to the VTA (arrows). Animals that have been exposed to formaldehyde (B) display increased fos (white) immunoreactivity in these neurons compared to control (ctrl) mice, which interacted with a novel object (C; Scale bars: 10 μm).
(D) Bar graph showing a significant increase in total number of fos-immunopositive cells in the LH of animals exposed to formaldehyde (form) compared to ctrl animals (form: 333.8 ± 17.68 cells, n = 4 mice; ctrl: 149.3 ± 17.92 cells, n = 4 mice; *** p < 0.001, unpaired Student's t-test; data represent means ± SEM).
(E) Bar graph showing no significant difference in the mean number of retrogradely labeled tdT-positive LH neurons between animals exposed to form and ctrl animals (form: 47.46 ± 4.31%, n = 4 mice; ctrl: 44.18 ± 4.51%, n = 4 mice; p = 0.618, unpaired Student's t-test; data represent means ± SEM).
(F) Bar graph showing significant increase in fos-immunoreactivity in retrogradely labeled, tdT-positive LH neurons projecting to VTA in response to form exposure compared with ctrl

animals. Form exposure does not alter fos-immunoreactivity in retrogradely labeled, tdT-negative (i.e., putative GABA neurons) LH neurons projecting to VTA (form: tdT-pos. 18.76 ± 2.21%, tdT-neg. 7.70 ± 1.34%, n = 4 mice; ctrl: tdT-pos. 10.06 ± 1.39%, tdT-neg. 7.56 ± 0.97%, n = 4 mice; ** $p < 0.01$; two-way ANOVA with Holm-Sidak's post-hoc test; data represent means ± SEM).

Figure S8. Ablation of LH_{VGLUT2} neurons and fiber photometry in the vNAcMed, Related to Figure 8.
Bar graphs showing terminal activity (quantified as area under the curve, AUC) in the vNAcMed before (first shock trial, red) and after aversive conditioning (last shock trial, blue) for mice expressing mCherry (left bar graph; tone: first: 2.18 ± 1.41; last: 36.47 ± 4.45; shock: first: 63.1 ± 5.37; last: 44.73 ± 7.85, n = 4 mice, two-way RM ANOVA, p(interaction) < 0.001 with Holm-Sidak post-hoc test, p(tone) = 0.003, p(shock) = 0.022) or Caspase 3 (CASP, right bar graph; tone: first: 2.19 ± 2.44; last: -4.01 ± 4.5; shock: first: 65.28 ± 5.18; last: 26.19 ± 9.97, n = 4 mice, two-way RM ANOVA, p(interaction) = 0.038 with Holm-Sidak post-hoc p(tone) = 0.506, p(shock) = 0.009) in LH_{VGLUT2} neurons (data represent means ± SEM). Note that the reduction in response to foot shock after aversive conditioning in Figure 1H is slightly more pronounced, which could reflect the differences between recordings in head-fixed versus freely-moving animals. Although the foot shock had the same intensity (0.4 mA) and duration (2 sec), it may be more aversive when administered in a head-fixed setup, since it is unescapable (i.e., by jumping, as shown see Supplementary Video 1).

Supplementary Tables

Supplementary Table 1. Quantification of monosynaptic rabies virus tracing, Related to Figures 3 and 6.
(A) Quantification of presynaptic input in different brain structures to vNAcMed-projecting DA neurons or NAcLat-projecting DA neurons.
(B) Quantification of *in situ* hybridization (ISH) experiments for cells in the LH, which express VGLUT2 and synapse onto different VTA cell populations.

Supplementary Movies

Supplementary Movie 1. Simultaneous *in vivo* fiber photometry recordings of dopamine terminals in the ventral NAcMed and NAcLat during the tone-shock conditioning paradigm (Related to Figure 1; Note that the orange line indicates duration of tone, while the blue line refers to the foot shock).

Supplementary Movie 2. Representative example (2x speed) showing optogenetic stimulation of LH_{VGLUT2} terminals in the VTA during the real-time place aversion assay (Related to Figures 4A-4F).

Supplementary Movie 3. Representative example showing optogenetic inhibition of LH_{VGLUT2} terminals in the VTA during the formaldehyde approach/avoidance assay (Related to Figures 4G-4M; left: control; right: NpHR).

Supplementary Movie 4. *In vivo* fiber photometry recordings of LH_{VGLUT2} terminals in the VTA during the formaldehyde approach/avoidance assay (Related to Figures 5A-5I; 5x speed, note that the speed of the video is intentionally decreased to 0.5x when the mouse approaches the formaldehyde stimulus).

Figure S1 de Jong, Afjei et al.

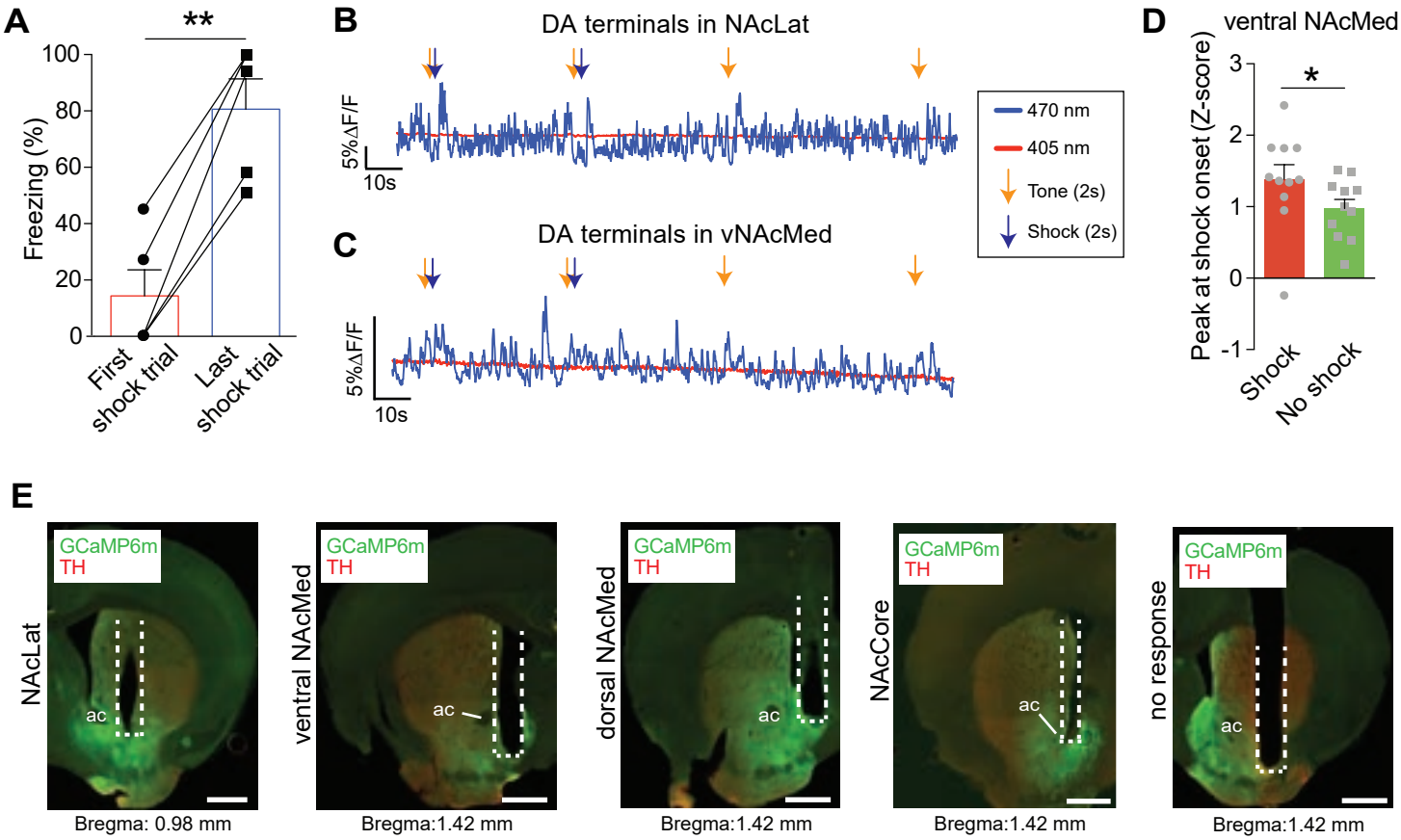

Figure S2 de Jong, Afjei et al.

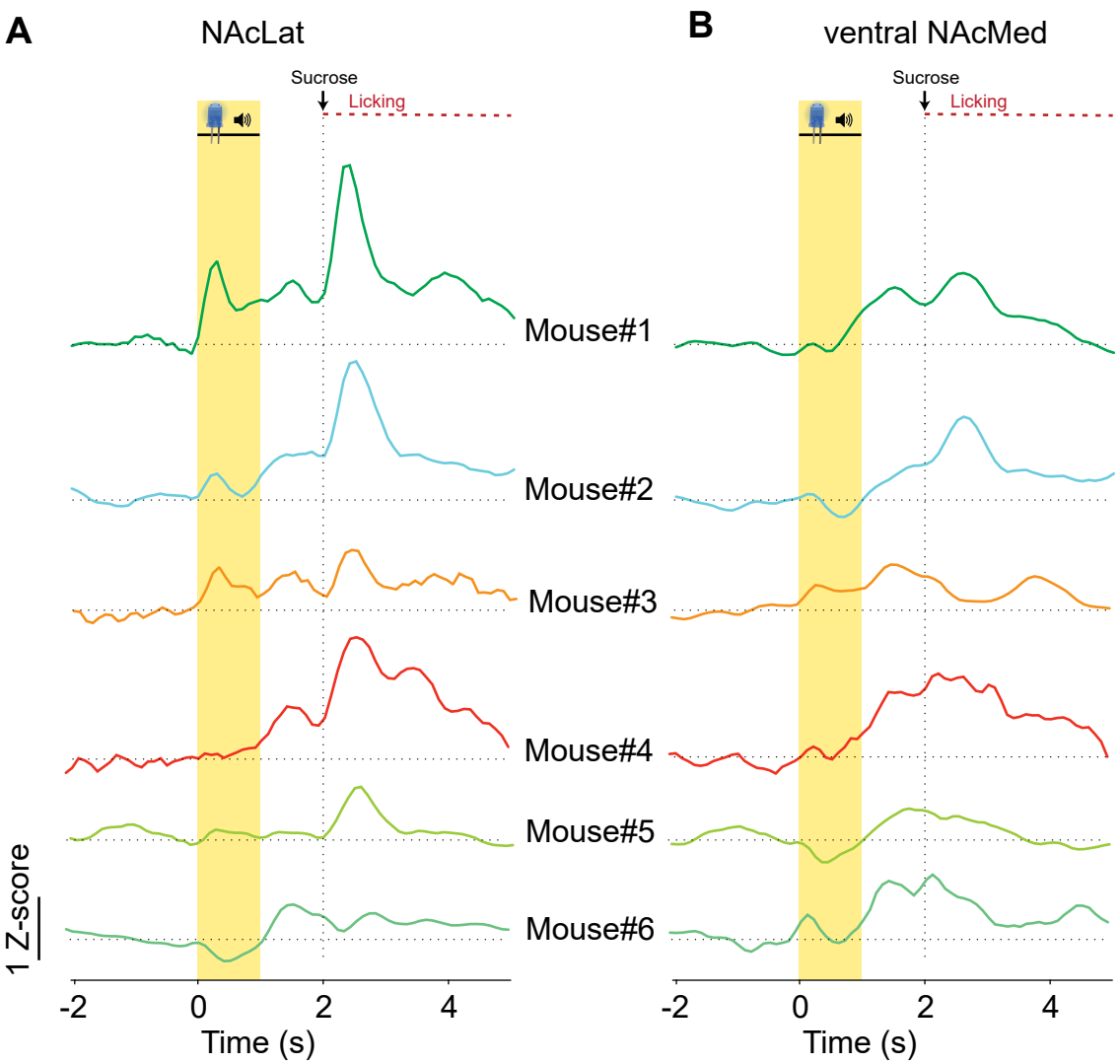

Figure S3 de Jong, Afjei et al.

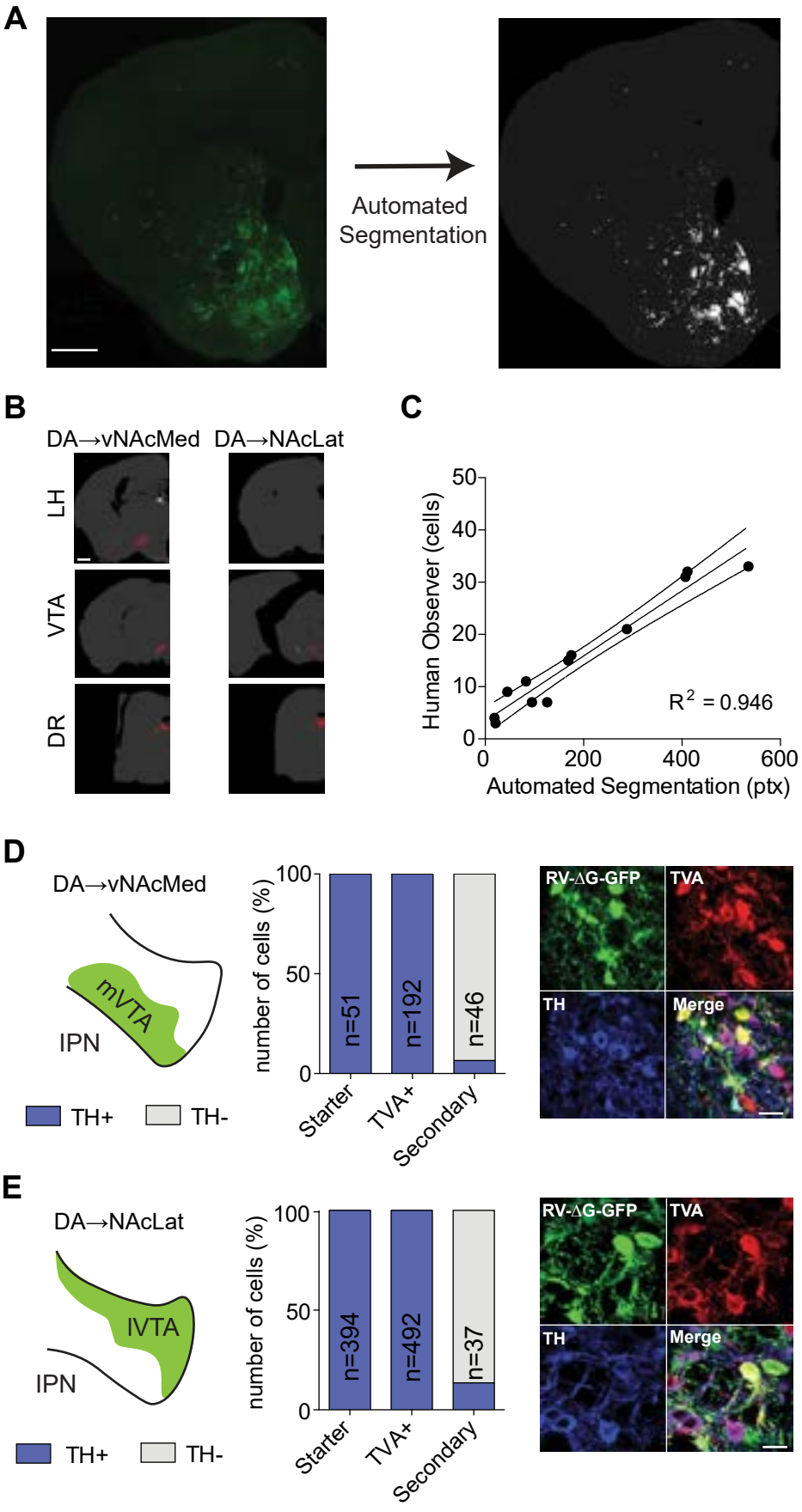

Figure S4 de Jong, Afjei et al.

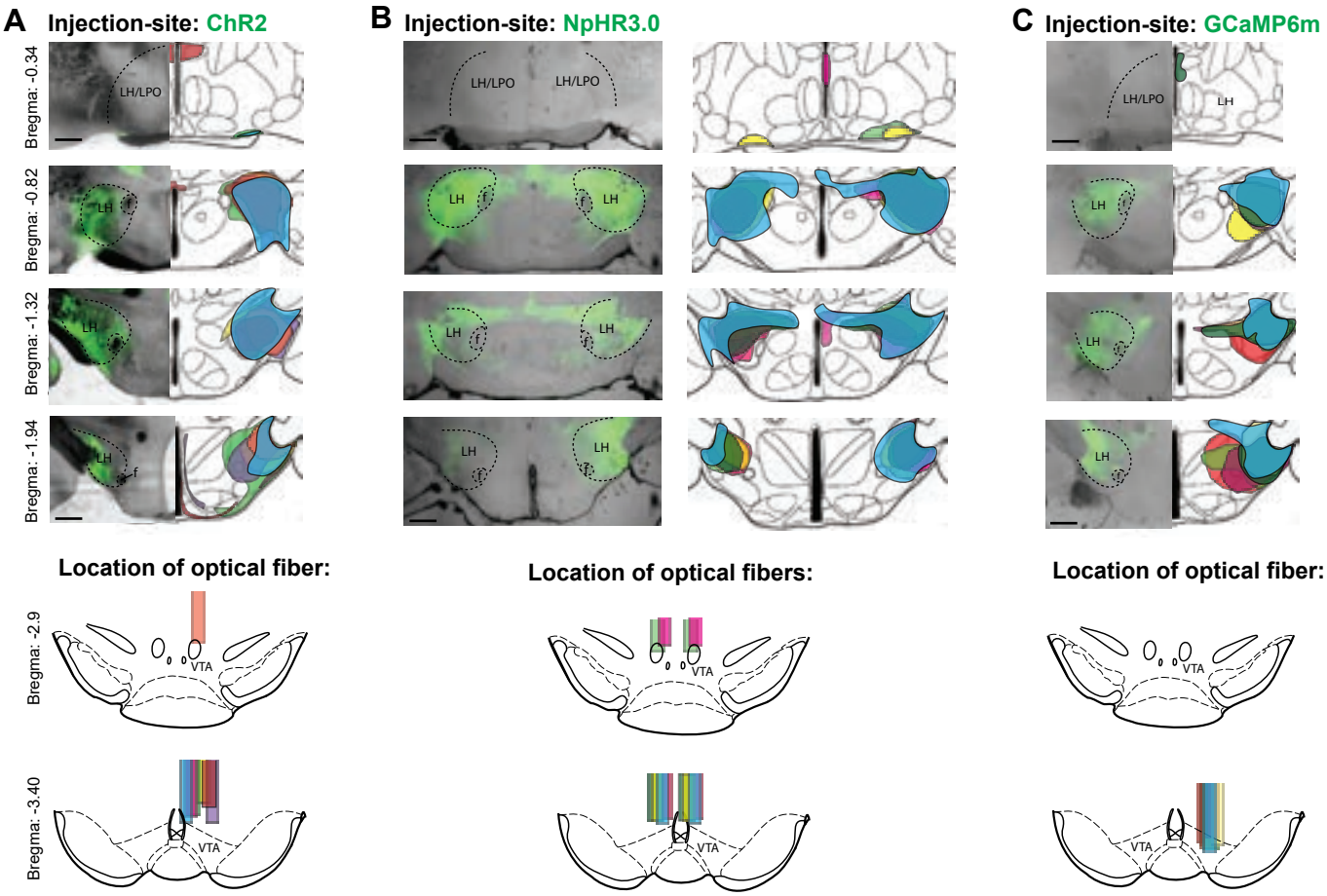

Figure S5 de Jong, Afjei et al.

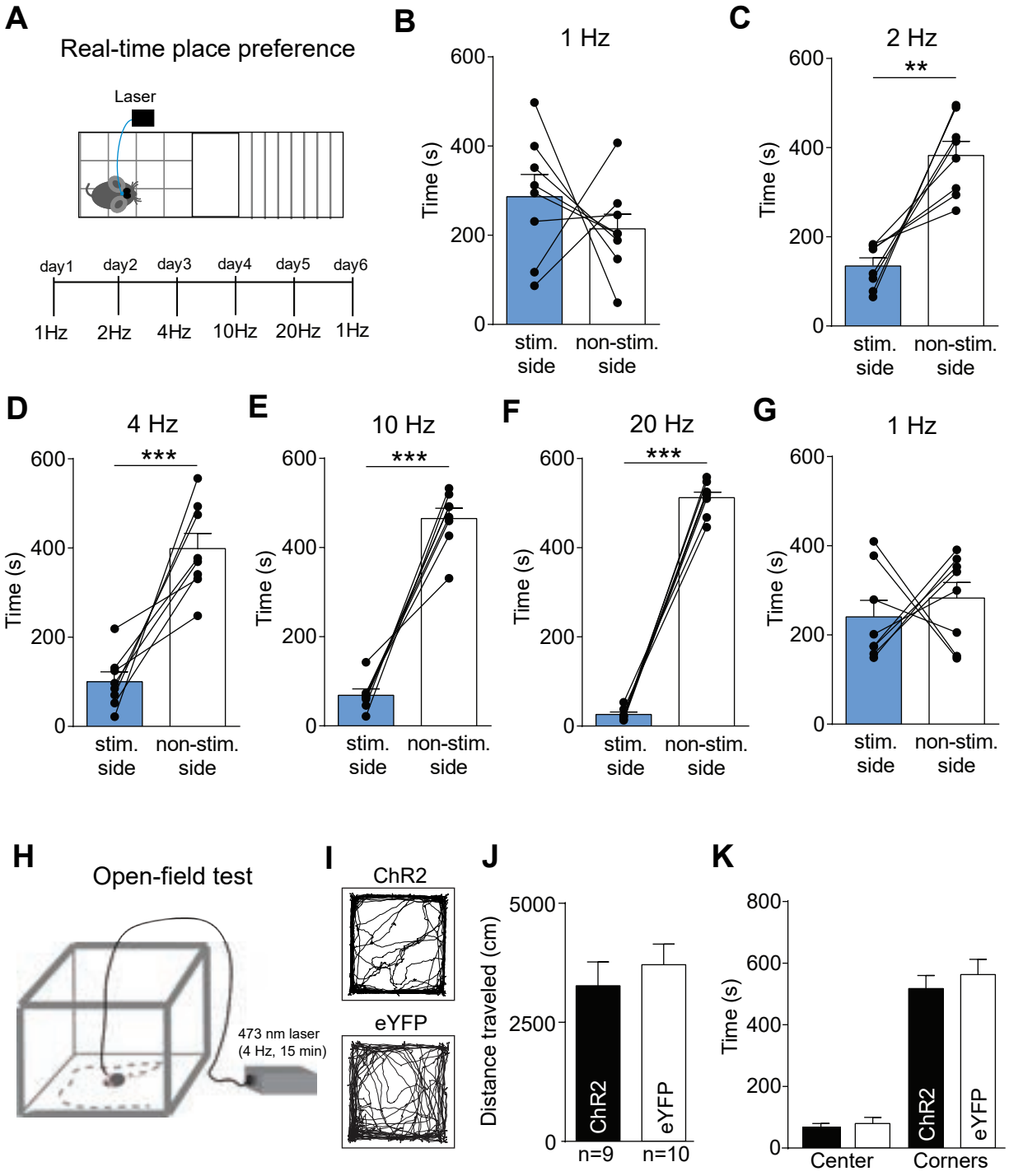

Figure S6 de Jong, Afjei et al.

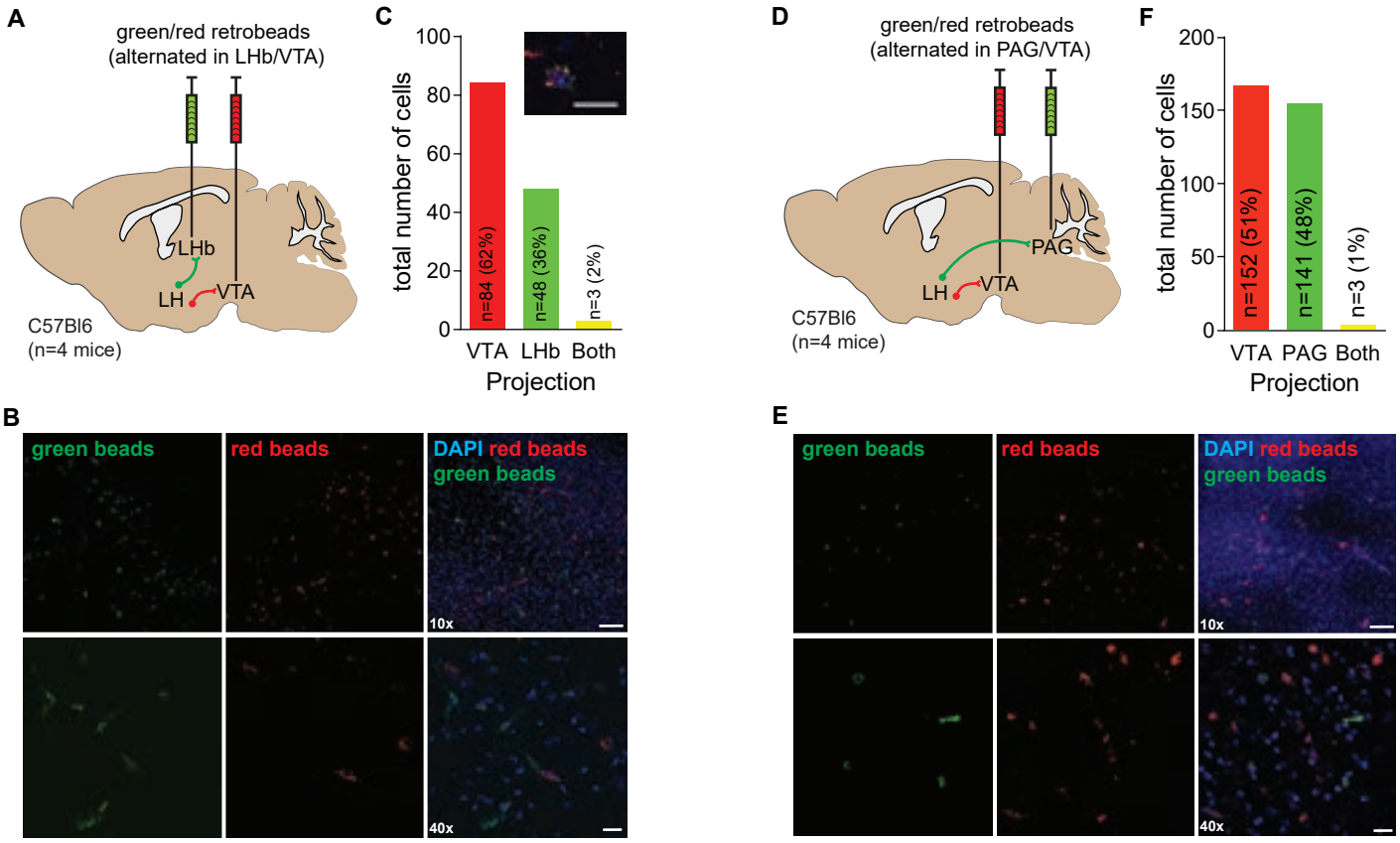

Figure S7 de Jong, Afjei et al.

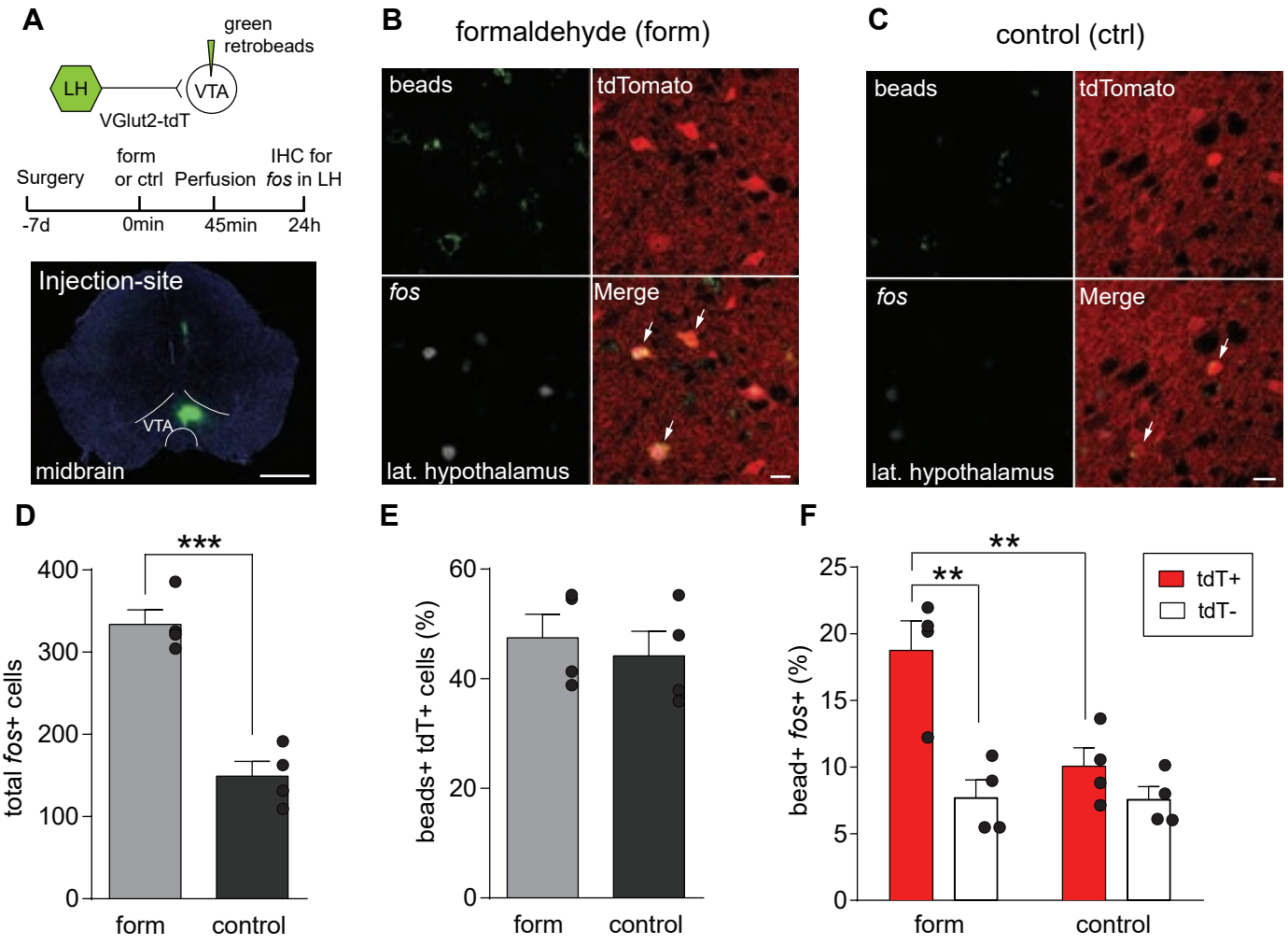

Figure S8 de Jong, Afjei et al.

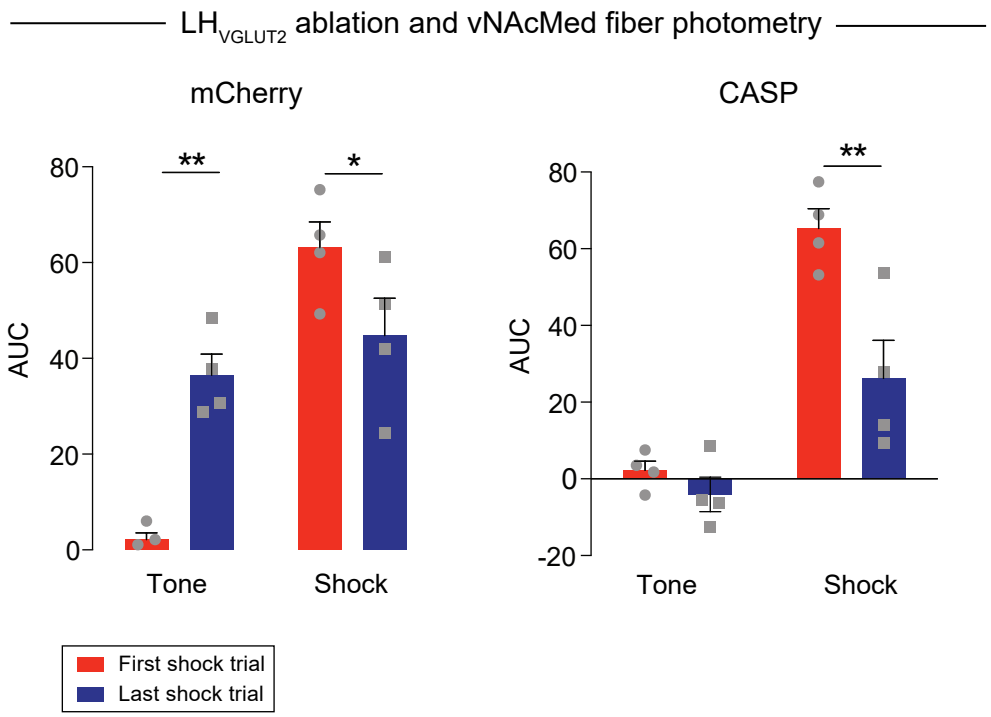

Supplementary Table 1 de Jong, Afjei et al.

A

	N	Total	VTA	Presynaptic Input (px) OFC	mPFC	DMS	DLS	NAcCore	NAcMed	NAcLat	VP	BNST	GP
VTA_{DA}→vNAcMed	4	136764 ± 65337	36143 ± 14256	619 ±519	992 ±654	220 ±134	3 ±2	2883 ±2576	9113 ±5702	630 ±410	10857 ±7864	2607 ±2155	480 ±381
VTA_{DA}→NAcLat	5	92106 ±63107	31861 ±18762	258 ±205	238 ±183	1157 ±918	22 ±15	2078 ±1529	4216 ±3456	1479 ±1229	5454 ±3602	2196 ±1853	1197 ±958

Presynaptic Input (px) PO	LH	PVN	CeA	LHb	MHb	STh	DR	LDT	LPB
1896 ±1483	17112 ±9392	1308 ±842	1052 ±843	2897 ±1525	447 ±267	373 ±233	42801 ±21728	3648 ±1854	686 ±424
303 ±180	10519 ±8132	596 ±414	1242 ±1083	319 ±170	65 ±44	515 ±275	26603 ±19232	1228 ± 788	559 ±541

B

Projection:	N	Avg. Labeled Cells	ISH+
VTA_{DA}→vNAcMed	3	259 ±32.1	88 ±9.0
VTA_{DA}→NAcLat	3	94 ±5.8	24 ±1.2
VTA_{GLUT}→vNAcMed	3	160 ±27.5	43.3 ±11.9
VTA_{GABA}	2	12.5 ±5	3.5 ±2